Highlights

Flow around tandem rough cylinders: effects of spacing and flow regimes

Raphaël Dubois,Thomas Andrianne

- Static tandem cylinders are investigated from sub- to post-critical regimes.
- Transition is promoted by adapted surface roughness.
- Unsteady pressure data give access to fluctuating and frequency features of the flow.
- Several spacing ratios are considered: $L/D = 1.2$, 1.4, 1.56 and 1.8.
- Identification of the flow patterns is made based on the unsteady pressure fields on the two cylinders.
- Eddy shedding is identified in the Strouhal range $0.13 < St < 0.32$, depending on the Reynolds number and spacing ratio.

Flow around tandem rough cylinders: effects of spacing and flow regimes

Raphaël Dubois[a,*], Thomas Andrianne[a]

[a]Department of Aerospace and Mechanical Engineering, University of Liège, Allée de la Découverte 9, 4000 Liège, Belgium

ARTICLE INFO

Keywords:
Two tandem circular cylinders
Wind tunnel
Unsteady pressure measurements
Flow regimes
Surface roughness

ABSTRACT

The aerodynamic features of the flow around static tandem cylinders are investigated in different flow regimes with the Reynolds number ranging from 21k to 395k. Adapted surface roughness ($k/D = 7.2 \times 10^{-3}$) is used to promote the transition from laminar to turbulent conditions in a low-subsonic wind tunnel. The effect of roughness on the mean force coefficients is investigated and a special attention is given to the uniformity of the roughness level along the span-wise dimension of the cylinders. Different spacing ratios are tested (L/D = 1.2, 1.4, 1.56 and 1.8). The measured unsteady pressure distributions are analysed and discussed for the different flow regimes as a function of the spacing ratio. The frequency content of the pressure fields is analysed in the range $0 \leq St \leq 0.75$ and eddy shedding phenomenon is identified for $0.13 < St < 0.32$ (including first harmonics) depending on the Reynolds number and the spacing ratio. In the sub- and critical regimes, it is shown that the flow belongs to the re-attachment pattern in which the shear layers re-attach either alternately or steadily, respectively. In the post-critical regime, the flow pattern is unstable for $1.2 \leq L/D \leq 1.56$ because of the intermittent re-attachment of the shear layers. For $L/D = 1.8$, the shear layers re-attach steadily.

1. Introduction

Because cylinder-like structures can be found in various engineering applications, fluid flows around circular cylinder have been extensively studied in the past and correspond to canonical problems in fluid mechanics. Air- or water-flows around single or multiple circular cylinders occur in the case of heat exchangers, chimneys, power lines, buildings, offshore structures, struts, landing gears, cables, etc. In many of these applications, several phenomena such as the eddy shedding or negative aerodynamic damping are responsible for flow-induced vibrations which can lead to stability issues. Therefore, a complete understanding of the flow is required at the design stage of such structures. The fundamental flow features around circular cylinder consist in boundary layers, separation, separated shear layers, re-attachment, dynamics of eddies and wake. Because of the significant interaction of transition from laminar to turbulence with the separation and boundary layer development, the flow around circular cylinders exhibits a strong Reynolds number dependency. Several comprehensive reviews of the flow around a single, isolated circular cylinder exist in the literature and are summarised in Zdravkovich (1997).

The effects on the flow when placing another circular cylinder in the proximity of the single circular cylinder have been investigated to a lesser extent. Side-by-side and staggered configurations have been respectively studied by Bearman and Wadcock (1973) and Sumner, Price and Païdoussis (2000), among others. The present work focuses on the tandem arrangement (see Fig. 1). The flow field becomes more intricate because of the interactions between the shear layers, eddies and wake. One of the earliest experimental studies on tandem cylinders has been carried on by Biermann and Herrnstein (1933) who studied the interference of airplane struts. They noticed that the presence of a cylinder in the wake of another one affects slightly the drag of the front cylinder (upstream) while the drag of the rear cylinder (downstream) is significantly reduced in comparison to the one acting on a single cylinder.

Zdravkovich (1987) classified the flow behaviour into three regimes based on the centre-to-centre spacing ratio L/D: (i) the extended-body regime, where $1 < L/D < 1.2-1.8$, the free shear layers separated from the front cylinder do not re-attach on the rear cylinder and they form a single vortex street behind the tandem arrangement; (ii) the re-attachment regime, where $1.2 - 1.8 < L/D < L_c/D$ with L_c being the critical spacing, the separated shear layers from the front

*Corresponding author.
raphael.dubois@uliege.be (R. Dubois)
ORCID(s): 0000-0002-7539-8362 (R. Dubois)

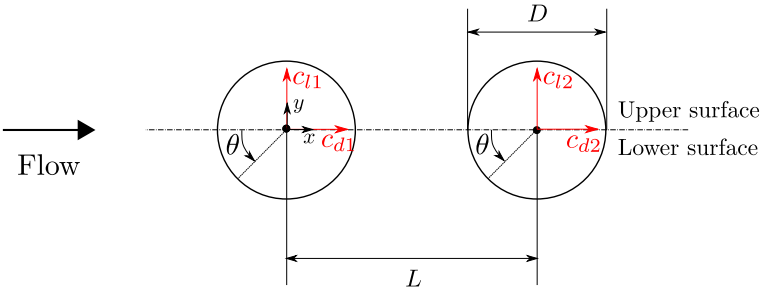

Figure 1: Two circular cylinders in tandem configuration in cross-flow.

cylinder re-attach on the rear cylinder and a vortex street is formed only behind the latter; (iii) the co-shedding regime, where $L/D > L_c/D$, the separated shear layers roll up alternatively, forming a vortex street between the front and the rear cylinders and both cylinders generate vortices. The spacing ratios corresponding to the transition from one regime to the other depend on several parameters such as the Reynolds number, the turbulent intensity (Ljungkrona, Norberg and Sunden, 1991; Lin, Yang and Rockwell, 2002) and the surface roughness. Igarashi (1981) suggested a similar classification where the second regime was divided into four different sub-regimes. Alam, Moriya, Takai and Sakamoto (2003) showed that the fluctuating fluid forces on the rear cylinder are highly sensitive to the spacing between the cylinders, especially below the critical spacing ratio.

Sumner (2010) and more recently Zhou and Alam (2016) reviewed the works on two circular cylinders in a cross-flow. Most of the previous studies on tandem cylinders have been performed in the sub-critical flow regime, i.e. Reynolds numbers below a critical value at which the drag crisis occurs. They revealed that the interference between the cylinders has a strong effect on the flow topology and varies with the centre-to-centre spacing ratio L/D and the Reynolds number Re.

The question then arises as to what happens at different flow regimes, i.e. in the super- and post-critical regimes or when approaching the fully-turbulent flow regime. Okajima (1979) was the first to experimentally simulate the post-critical flow regime around cylinders in tandem arrangement by means of surface roughness. He investigated the variation of the time-averaged drag coefficients and Strouhal numbers of both individual cylinders with the Reynolds number and spacing ratio. Sun, Gu, He and Zhang (1992) studied the super-critical flow regime and stated that the interference effects of two neighboring cylinders are weaker than that in the sub-critical regime. A recent investigation on the flow around tandem smooth cylinders from sub- to post-critical regimes has been conducted by Schewe and Jacobs (2019) in a high-pressure wind tunnel. It consists in a parametric analysis of time-averaged flow quantities for a given spacing ratio ($L/D = 1.56$). Undesired vibrations of the static set-up were reported in the post-critical regime. The authors concluded that the strong non-linearity of the force and moment coefficients is heavily dependent on the Reynolds number and is responsible for the difficulty to identify the source(s) of excitation of the flow-induced vibrations. Furthermore, they support the need to measure unsteady forces in order to better understand the different types of flow-induced vibrations.

The present work consists in experimental measurements of the unsteady flow field around tandem cylinders from sub- to post-critical regimes. It is based on the use of surface roughness, as successfully done by Okajima (1979), to reach the post-critical flow regime at lower Reynolds numbers in the low-subsonic wind tunnel of the University of Liège. The effects of the surface roughness on the flow around a single circular cylinder have been thoroughly investigated in the past (Fage and Warsap, 1929; Achenbach, 1971; Szechenyi, 1975; Güven, Farell and Patel, 1980; Adachi, 1997; van Hinsberg, 2015). The main effect of the surface roughness is to promote the transition from laminar to turbulence and hence to decrease the critical Reynolds number at which the drag crisis phenomenon takes place. Consequently, it allows to go beyond the critical flow regime and reach the fully-turbulent regime at lower Reynolds numbers. Through this methodology, the regimes from sub- to post-critical are reached and studied within the tested Reynolds number range. In this work, the use of surface roughness is deeply investigated and discussed. It is important to remember that the experimental results and conclusions about the different phenomena observed are limited to the tested roughness levels and Reynolds numbers.

Four different centre-to-centre spacing ratios L/D, which are all below the critical spacing ratio, have been tested. The resulting flow behaviours all belong to the second regime defined by Zdravkovich (1987), i.e. the re-attachment regime. The effects of the spacing ratio on the flow field in this particular range are discussed. Experiments consist in unsteady pressure measurements at the mid-span of both cylinders. The two-dimensional pressure forces acting on the cylinders, which are presented in this work, are computed by integrating the pressure along the surface.

2. Experimental methodology

2.1. Wind tunnel

The experimental campaign is performed in the wind tunnel facility of the University of Liège. This facility consists in a closed-loop low-subsonic wind tunnel. The aeronautical test section in which the model is mounted is 2 m in width and 1.5 m in height. In this study, the windspeed varies from 2.5 m/s to 47 m/s and the flow is characterised by a low level of turbulence (maximum turbulence intensity of 0.2%).

2.2. Model

The experimental model, shown in Fig. 2, consists in cylinders with an external diameter D of 0.125 m and a span length S equal to 1.25 m. This leads to an aspect ratio and a geometric blockage ratio equal to 10 and 6.25%, respectively. The value of the blockage ratio being lower than 10%, no correction is applied as it is common practice in similar wind tunnel tests. The tested Reynolds number Re based on the external diameter D is therefore ranging from 21k[1] to 395k. The cylinders arranged in tandem are clamped on both sides using end-plates to minimize the three-dimensional effects. Each cylinder is composed of two parts: an instrumented central part obtained by means of a 3D printing technique which allows to control the surface roughness near the measurement locations and steel parts on the extremities covered by sandpapers. The same equivalent surface roughness is used on the two parts. The set-up is mounted vertically on a turn-table, allowing to adjust accurately the angle of attack of the cylinders with respect to the incoming flow. In this work, the angle of attack is set to 0 degree for all configurations to obtain the tandem arrangement. The cylinder centre-to-centre spacing ratio L/D can be varied by moving forward or backward the rear cylinder by means of pre-defined holes drilled on the end-plates. It leads to investigated spacing ratios of 1.2, 1.4, 1.56 and 1.8. The spacing ratio of 1.56 (instead of 1.6) is used to compare the present results with the ones of Schewe and Jacobs (2019). The experimental model is intended to be static and was designed in order to minimize the structural vibrations. This is performed by using steel tubes with large stiffness. For all tests presented in this study no vibration was observed.

Figure 2: Picture of the experimental model installed in the aeronautical section of the wind tunnel of ULiège.

[1] k stands for "thousand".

2.3. Instrumentation

Each cylinder is instrumented by 48 pressure taps of 1 mm in inner diameter, equally spaced on an instrumented section at the mid-span. Pressure is measured during 60 seconds at a sampling frequency of 600 Hz using a pressure scanner (from Turbulent Flow Instrumentation Pty Ltd) with a range of ±2.7 kPa and accuracy of ±0.5 % of the full-scale. Dynamic effects of the pressure lines are corrected using the analytical model by Bergh and Tijdeman (1965). The pressure coefficient C_p is calculated using

$$C_p(t) = \frac{p(t) - p_\infty}{1/2\rho U_\infty^2} \tag{1}$$

where $p(t)$ is the cylinder surface pressure measured by the pressure scanner and p_∞ is the static pressure measured at the free-stream reference which is located at x/D=-4.36 and y/D=-2.64, as seen in Fig. 2. The origin of the x-coordinate is located in the centre of the front cylinder (Fig. 1). The Pitot tube provides the dynamic pressure ($1/2\rho U_\infty^2$) allowing to extract the flow velocity U_∞ in the wind tunnel.

The time-dependent pressure components of two-dimensional lift coefficient c_l and drag coefficient c_d are obtained by integrating the surface pressure,

$$c_l(t) = \frac{1}{2}\int_0^{2\pi} C_p(t)\sin(\theta)d\theta, \tag{2}$$

$$c_d(t) = \frac{1}{2}\int_0^{2\pi} C_p(t)\cos(\theta)d\theta, \tag{3}$$

where θ is the angular position from the leading stagnation point of the cylinder, as shown in Fig. 1. In the present work, C_p' and c_l' correspond to the standard deviation of the pressure and lift coefficients, respectively.

2.4. Use of surface roughness

A careful preliminary investigation is performed on a single cylinder in order to validate the use of surface roughness to access critical and post-critical flow regimes. To this end, four different surface roughnesses for the instrumented central part of the cylinder are investigated. The parameters of the generated surface roughnesses are given in Table 1 and defined in Fig. 3. Three different regular patterns of cubic excrescences are used (see Fig. 4).

Table 1
Description of the different generated surface roughnesses of the central part.

Name	k/D	Pattern	c_{lx_r}/D	Density (2D)	S_q/D
A1	7.2×10^{-3}	A	1.6×10^{-2}	25%	3.1×10^{-3}
A2	1.1×10^{-2}	A	1.6×10^{-2}	25%	4.9×10^{-3}
B	7.2×10^{-3}	B	1.6×10^{-2}	50%	3.6×10^{-3}
C	7.2×10^{-3}	C	1.6×10^{-2}	25%	3.1×10^{-3}

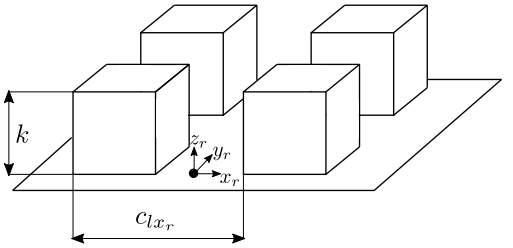

Figure 3: Definition of the parameters of the printed surface roughnesses on the central part of the cylinder (Pattern A is shown here).

Pattern A corresponds to cubic excrescences aligned with the free-stream with a two-dimensional surface density equal to 25%. This density is increased to 50% to obtain pattern B (chessboard-like pattern). Finally, the excrescences

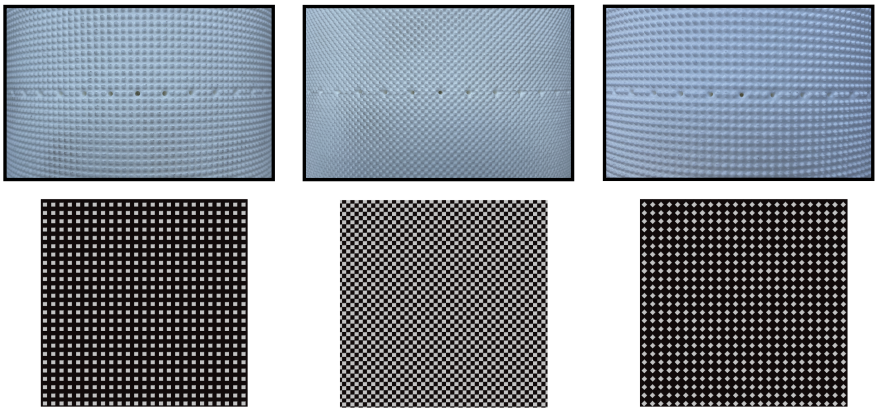

(a) Pattern A (b) Pattern B (c) Pattern C

Figure 4: Description of the different roughness patterns printed on the central part of the cylinder.

from the first pattern are rotated by an angle of 45° to obtain pattern C. The relative height of the excrescences k/D is kept the same for all surface roughnesses except for A2 where it is slightly increased. The relative periodicity length in the stream-wise direction c_{lx_r}/D remains the same for each surface roughness. The parameter S_q corresponds to the two-dimensional standard deviation of the surface defined by

$$S_q = \sqrt{\frac{1}{A}\iint_A z_r^2(x_r, y_r)\, dx_r\, dy_r}. \tag{4}$$

In this expression, z_r is the height-coordinate of the surface from its averaged value. Thus, S_q depends on both k/D and the pattern.

2.4.1. Effect of the central roughness

Fig. 5 shows the variations of the time-averaged drag coefficient c_d and lift coefficient c_l of a single circular cylinder with the Reynolds number for different surface roughnesses on the instrumented central part. Sandpaper P40 (ISO/FEPA) is applied on the rest of the cylinder for each tested central roughness. Surface roughness A1 is taken as the reference. The relative height k/D of this surface roughness is intentionally high ($k/D = 7.2 \times 10^{-3}$) in order to reach the post-critical flow regime within the accessible Reynolds numbers of the wind tunnel.

For roughness B, the two-dimensional surface density is increased to 50% and the drag coefficient curve remains similar. The critical flow regime, which is characterised by the drag crisis and a non-zero lift coefficient, is slightly shifted to lower Reynolds numbers. The critical regime with roughness A1 begins at Re $\approx$ 65k while it begins at Re $\approx$ 60k with roughness B. Beyond that critical regime, i.e. Reynolds number above 100k, the drag coefficient with the roughness B is found to be slightly smaller than with roughness A1. This difference is lower than 10%.

For roughness C, the cubic excrescences are rotated by 45° and the drag coefficient curve remains similar to the ones of roughnesses A1 and B. The critical regime is slightly shifted to lower Reynolds numbers in comparison with the roughness A1. Similarly to the configuration with roughness B, it begins at Re $\approx$ 60k. When the Reynolds number is increased (Re $>$ 80k), the drag coefficient with roughness C is found to be equal to the one with roughness A1.

The drag coefficient curve is rather different for roughness A2 which is characterised by a larger relative height of the excrescences ($k/D = 1.1 \times 10^{-2}$). The occurrence of the drag crisis and non-zero lift coefficient is observed at a significantly lower Reynolds number. The critical regime begins at Re $\approx$ 47k. Based on the literature, this observation is expected from an increase of the relative height of the surface roughness. Nonetheless, it is observed that the drag coefficient decreases in two steps with roughness A2 in the critical regime: a first step between Re $\approx$ 47k and Re $\approx$ 60k and a second one between Re $\approx$ 60k and Re $\approx$ 75k. It is attributed to span-wise effects discussed in the next section. At larger Reynolds numbers (Re $>$ 80k), the drag coefficient is nearly the same but slightly larger than with roughness A1.

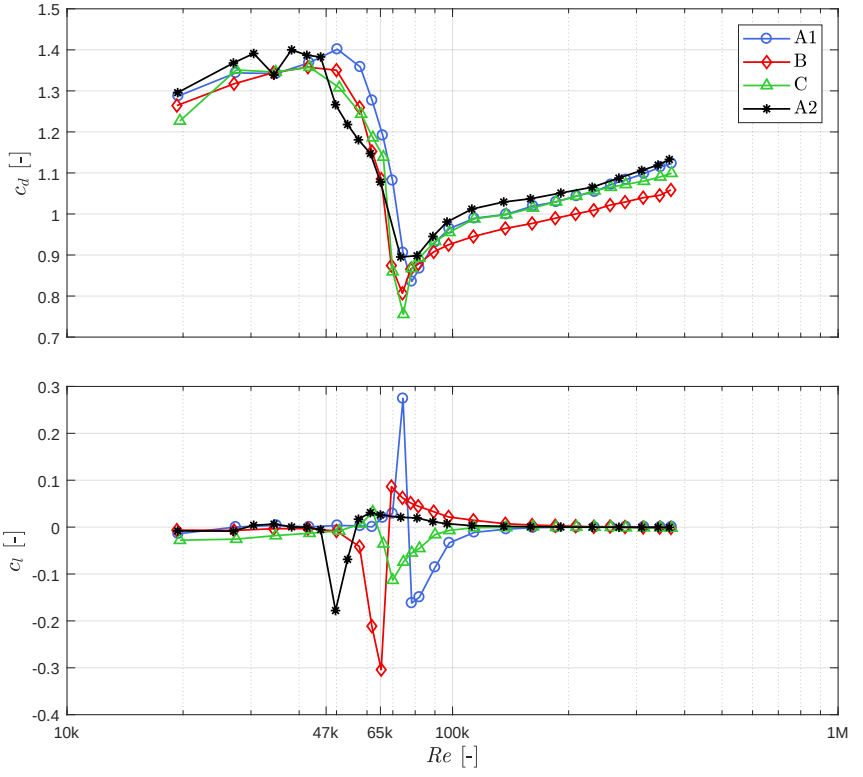

Figure 5: Variation of the time-averaged drag coefficient c_d and lift coefficient c_l of a single cylinder with Re for different printed surface roughnesses and sandpaper P40 applied on the extremities of the cylinder.

Based on these observations, it is concluded that the pattern of the central roughness has a very limited influence on the flow at the measurement section. Therefore, the pattern A is retained for the rest of the tests. On the other hand, it is shown that the parameter k/D has a strong effect: the drag crisis occurs earlier for larger k/D. However, the results with the roughness A2 reveal span-wise effects. The surface roughness A1 is selected to perform the experimental campaign on the tandem cylinders.

2.4.2. Effect of the span-wise roughness

The effect of the span-wise roughness (sandpaper applied on the rest of the cylinder) is investigated with the surface roughness A1 for the central part. Three different roughness levels are considered: no sandpaper ($k/D = 10^{-4}$), sandpaper P24 ($k/D = 1.2 \times 10^{-2}$) and sandpaper P40 ($k/D = 6.7 \times 10^{-3}$).

The variations of the time-averaged aerodynamic force coefficients of a single cylinder with the Reynolds number for the different span-wise roughnesses are shown in Fig. 6.

A unique drag crisis is observed when applying sandpaper P40. It is interesting to notice that a drag crisis begins at Re $\approx$ 65k for each configuration. This drag crisis is inferred to correspond to the critical flow regime on the central part of the cylinder with roughness A1. It is corroborated by the simultaneous occurrence of a non-zero lift coefficient which characterises the critical regime.

Without sandpaper or with sandpaper P24, two drag crises are observed in the drag coefficient curve. The second drag crisis observed in this cases corresponds to the occurrence of the critical regime on the extremities of the cylinders. Without sandpaper, it begins at a larger Reynolds number (Re $\approx$ 250k) because the roughness of the steel is much lower than roughness A1. The roughness of sandpaper P24 is, conversely, larger than the roughness A1, hence the second drag crisis begins at a lower Reynolds number (Re $\approx$ 30k).

It is concluded that the span-wise roughness has a strong effect on the flow at the measurement section. Non-equivalent surface roughnesses on the central part or the rest of the cylinder give rise to undesired span-wise effects,

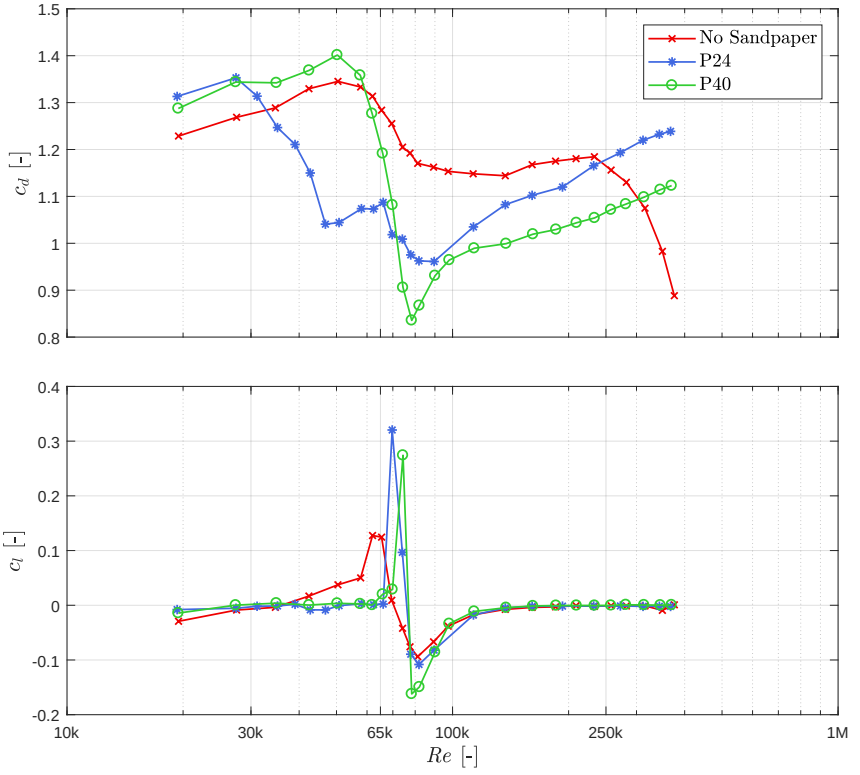

Figure 6: Variation of the time-averaged drag coefficient c_d and lift coefficient c_l of a single cylinder with Re for the surface roughness A1 and different roughnesses applied on the extremities of the cylinder.

e.g. the occurrence of two drag crises. Based on this, it is assumed that the double drag crisis (see roughness A2 in Fig. 5) is due to the fact that roughness A2 and sandpaper P40 are not exactly equivalent. The unique drag crisis obtained with the combination of sandpaper P40 and roughness A1 indicates that their roughness is equivalent. This configuration (P40 + roughness A1) is used for the experiments on the tandem arrangement.

3. Results

The different flow regimes are first identified as a function of the Reynolds number on the basis of the aerodynamic force coefficients. Then, the pressure distributions on the cylinders are discussed. The nomenclature used to define the flow regimes around the tandem arrangement follows the one suggested by Zdravkovich (1997) for the flow around a single circular cylinder. The abbreviations 'SL' and 'BL' respectively stand for 'shear layers' and 'boundary layers'. The notation 'Tr' refers to the development of the transition from laminar to turbulent flow (either in the shear layers or the boundary layers) around the cylinders. In that sense, this work consists in the extension of the flow regimes around tandem rough cylinders.

3.1. Time-averaged drag and lift coefficients

The time-averaged drag and lift coefficients for both individual cylinders arranged in tandem are plotted against the Reynolds number in Fig. 7. The results from the single cylinder are superimposed on the ones of the front cylinder in order to assess the effect of the presence of a cylinder in its the wake.

The variation of the time-averaged drag coefficient of the front cylinder is very similar to the one of a single circular cylinder, as it can be seen in Fig. 7(a). Flow regimes around the tandem arrangement based on the Reynolds number can therefore be defined similarly to the ones around a single circular cylinder. By making use of the states of flow defined by Zdravkovich (1997), five flow regimes are observed in the tested Reynolds number range. Fig. 7(b) shows

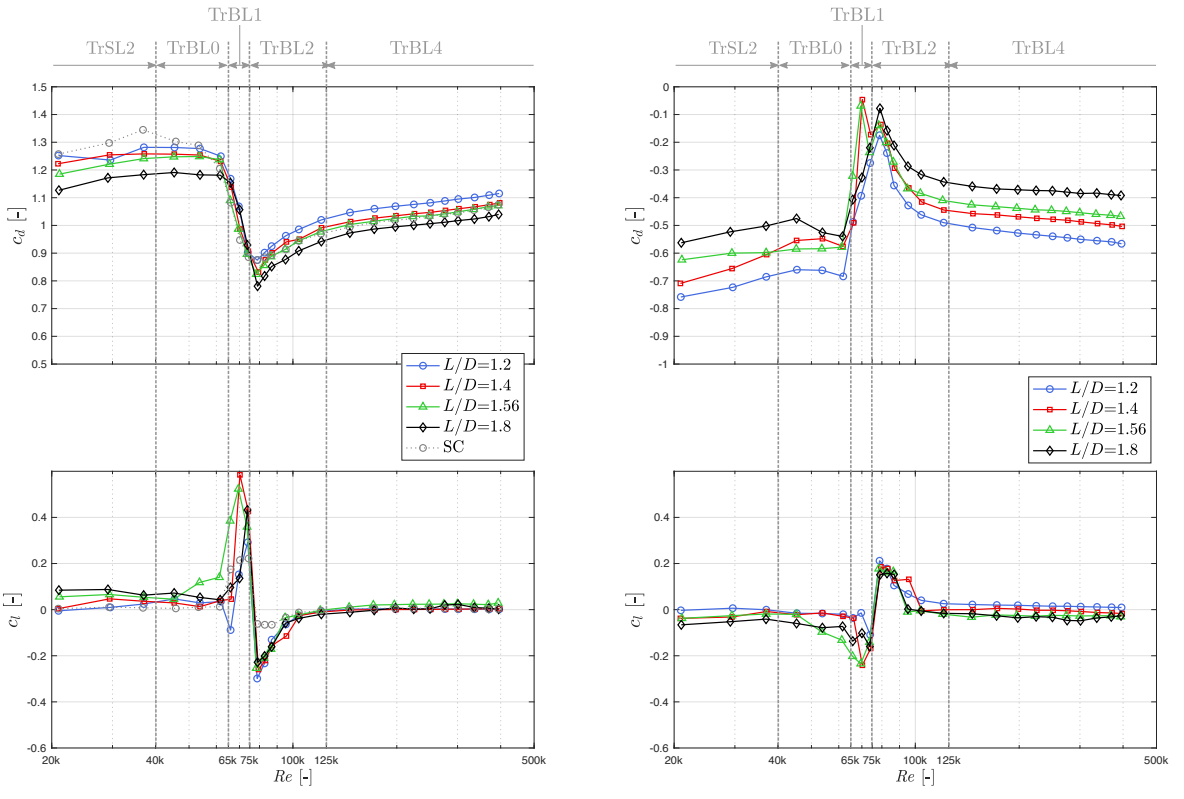

(a) Front cylinder (b) Rear cylinder

Figure 7: Variation of the time-averaged drag coefficient c_d and lift coefficient c_l with Re for different spacing ratios L/D.

that the time-averaged drag coefficient of the rear cylinder remains negative within the entire tested Reynolds number range and for each spacing ratio L/D. These negative values indicate that the spacing ratios are all below the critical spacing ratio: the flow belongs to the extended-body or re-attachment regimes defined by Zdravkovich (1987). Being in the wake of the front cylinder, the rear cylinder is pushed towards the former one. This negative drag force was observed by Okajima (1979) and Schewe and Jacobs (2019), among others.

It should be pointed out that the identification of the flow regimes based on a single circular cylinder is also applicable for the rear cylinder.

The first flow regime is called TrSL2 and belongs to the sub-critical state of flow. As suggests by the terminology, the transition from laminar to turbulence in this regime occurs in the separated shear layers of the front cylinder. In this regime, the time-averaged drag coefficients slightly increase for both cylinders and all spacing ratios when the Reynolds number increases. On the other hand, the time-averaged lift coefficients do not vary with the Reynolds number. Nonetheless, it is observed that the lift coefficients are not perfectly equal to zero. This may emanate from a slight misalignment of the cylinders with respect to the incoming free-stream in the wind tunnel. TrSL2 regime extends up to Re $\approx$ 40k.

It is followed by the so-called pre-critical TrBL0 flow regime (Morkovin (1964)). Unlike suggested by its name, the transition is not located in the boundary layers. Instead, the onset of transition in the free shear layers comes very close to the separation lines on the front cylinder so that the flow is slightly disturbed. This results in a very limited decrease of the time-averaged drag coefficients, as it is explained by Zdravkovich (1997) for a single cylinder. Except for $L/D = 1.56$, the lift coefficients remain more or less constant as it can be seen in Fig. 7. For $L/D = 1.56$, the lift coefficient of the front cylinder slightly increases while the one of the rear cylinder decreases. The pre-critical regime suddenly terminates at Re $\approx$ 65k.

The Reynolds number Re ≈ 65k marks the beginning of the TrBL1 flow regime. TrBL1 is called the critical regime because of the occurrence of the drag crisis within its Reynolds number range, as observed in Fig. 7(a). In this regime, the transition reaches the separation point on one side of the front cylinder only. The resulting turbulent boundary layer separation is considerably delayed. On the other side of the cylinder, the boundary layer remains laminar because the onset of transition has not reached the separation point yet and thus separates earlier. This leads to an asymmetry of the flow around the tandem arrangement, as observed for a single rough cylinder by van Hinsberg (2015). The asymmetric flow generates a positive lift force on the front cylinder and a negative one on the rear cylinder. In contrast to the decrease of the time-averaged drag coefficient of the front cylinder, the drag force acting on the rear cylinder increases with the Reynolds number in TrBL1.

The next regime, TrBL2, starts at Re ≈ 75k. Around this particular Reynolds number, the transition reaches the separation point on the other side of the front cylinder, i.e. where the boundary layer remained fully laminar at lower Reynolds numbers. Hence, the separation is strongly delayed. The resulting flow remains asymmetric. However, one can see in Fig. 7 that the asymmetry has changed sign in comparison with the preceding flow regime. Indeed, a negative lift force is acting on the front cylinder while the rear cylinder is pushed upward. As the Reynolds number is increased, the flow becomes more and more symmetric: the time-averaged lift coefficients converge towards zero. Simultaneously, the time-averaged drag coefficient of the front cylinder increases again and the one of the rear cylinder decreases.

The last identified flow regime is the post-critical TrBL4. It begins at Re ≈ 125k, when the flow around the tandem cylinders is symmetric again: the time-averaged lift coefficients are equal to zero in its Reynolds number range. The time-averaged drag coefficients of the front and rear cylinders are respectively increasing and decreasing with the Reynolds number in TrBL4. The end of TrBL4 corresponds to the beginning of the fully-turbulent flow regime.

It should be mentioned that the regimes TrBL1 and TrBL2 defined in the present work differ from the namesake regimes presented by Zdravkovich (1997). Indeed, the flow regimes TrBL1 and TrBL2 around a smooth circular cylinder are respectively called one-bubble and two-bubble regimes. They correspond to the formation a laminar separation bubble on one side of the cylinder for the former regime and the formation of a second bubble on the other side of the cylinder for the latter regime. The regimes represent an intricate combination of laminar separation, transition, re-attachment and turbulent separation of the boundary layers. One-bubble and two-bubble regimes, being very sensitive to disturbances, disappear if sufficient roughness is present on the surface. The flow regime TrBL3, also known as the super-critical regime, is also missing when using surface roughness. This regime corresponds to the disruption of the laminar separation bubbles on the span of the cylinder which leads the disorganization of the wake behind the front cylinder. However, no separation bubble is formed as it was just explained and the eddy shedding never ceases. Two flow regimes, namely TrBL1 and TrBL2, were nonetheless defined in this study between the pre- and post-critical flow regimes to take into account the different resulting asymmetric flows in this particular Reynolds number range.

Table 2 compares the time-averaged drag coefficients obtained by Schewe and Jacobs (2019) and the present ones for a spacing ratio $L/D = 1.56$. The three main flow regimes are considered: sub-critical, critical and post-critical flow regimes. Because of the different roughness levels between the work of Schewe and Jacobs (2019) and the present work, the flow regimes take place at different Reynolds numbers, as depicted in Table 2.

Table 2
Comparison of the drag coefficients obtained from the work of Schewe and Jacobs (2019) (k/D=10^{-4}) and the present one (k/D=7.2×10^{-3}) at different flow regimes for a spacing ratio $L/D = 1.56$.

Work	Cylinder	sub-critical		critical		post-critical	
Schewe and Jacobs (2019)	Front	Re=200k	1	Re=500k	0.05	Re=6M	0.5
	Rear		-0.4		0.4		-0.07
Present work	Front	Re=45k	1.25	Re=79k	0.82	Re=395k	1.08
	Rear		-0.6		-0.14		-0.46

In the sub-critical flow regime, the absolute value of each drag coefficient increases with the surface roughness. It is expected for the front cylinder. Indeed, the surface roughness reduces the momentum in the boundary layers which results in an upstream displacement of the separation points, leading to an increase of the drag coefficient (Güven et al. (1980)). The upstream displacement of the separation points from the front cylinder has the effect of widening its wake. It increases the « shielding » effect on the rear cylinder, reducing its drag coefficient.

The same observations and interpretations can be made in the post-critical flow regime. One can state that the effect of the surface roughness is more significant in the post- than in the sub-critical flow regime.

In the critical flow regime, it is considerably different: the drag coefficient of the front cylinder is significantly higher in presence of roughness. Moreover, the drag coefficient of the rear cylinder remains negative (-0.14) while it is positive (0.4) in Schewe and Jacobs (2019). The surface roughness prevents the formation of the laminar separation bubbles on the front cylinder which characterises the critical regime of a smooth cylinder. Therefore, the separation points move upstream in the critical regime with surface roughness, resulting in an increase of the drag coefficient of the front cylinder. As mentioned above, the width of the wake behind the front cylinder increases, hence decreasing the drag coefficient of the rear cylinder.

Based on this comparison, the flow around the tandem arrangement is not exactly the same for different roughness levels and Reynolds numbers although it is in the same flow regime. Therefore, if scaling is planned based on the present results, the reader should take care of the similarities regarding the Reynolds number and the roughness parameter k/D. They cannot be applied to smooth cylinders at high Reynolds numbers.

3.2. Fluctuating lift coefficients

Fig. 8 shows the variation of the fluctuating lift coefficient c_l' (standard deviation of the lift signal for each individual cylinder) with the Reynolds number.

The first observation concerns the reduction of the fluctuating lift coefficient of the front cylinder in comparison to the one of a single cylinder (Fig. 8(a)). This reduction is attributed to the presence of a cylinder in its wake. The flow belongs to the extended-body or re-attachment regimes, hence the eddies shed by the tandem arrangement are formed behind the rear cylinder and therefore have a lower influence on the flow around the front cylinder. In the sub-critical flow regime, the fluctuating lift coefficient of the rear cylinder is also lower than the one of a single cylinder. On the opposite, it is observed that it becomes larger for each tested spacing ratio in the post-critical regime (Fig. 8(b)).

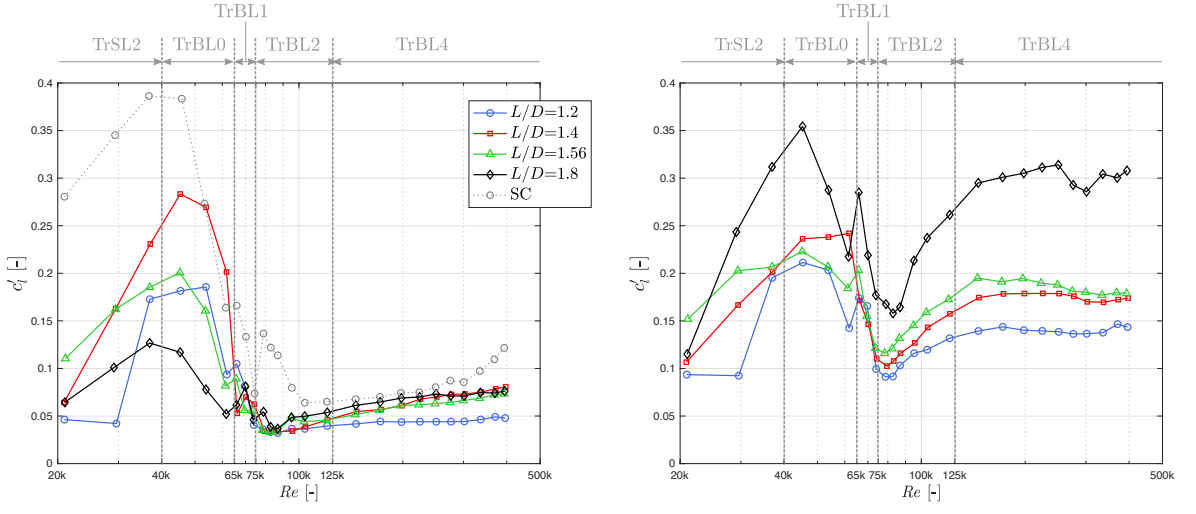

(a) Front cylinder (b) Rear cylinder

Figure 8: Variation of the fluctuating lift coefficient c_l' with Re for different spacing ratios L/D.

The fluctuating lift coefficients of both cylinders increase with the Reynolds number in the TrSL2 regime up to the beginning of the TrBL0 regime. This variation with the Reynolds number differs both in amplitude and shape for

the different spacings. It is difficult to extract a clear tendency in the variation of the fluctuating lift coefficients with the spacing ratio at the lowest Reynolds numbers. This may be caused by the small pressure fluctuations that were measured at those small flow velocities, leading to a larger contribution of the noise in the measurements.

When increasing the Reynolds number further in TrBL0 and TrBL1 regimes, the fluctuations on both cylinders drastically decrease and they reach their respective minimum value at the beginning of the asymmetric TrBL2 regime. A possible explanation involves the downstream movement of the separation points on the front cylinder induced by the transition from laminar to turbulent boundary layers. This delay of separation narrows the wake of the front cylinder and stabilises the flow between the cylinders, leading to smaller fluctuations. It is observed that the minimum value obtained for the rear cylinder is larger than the one for the front cylinder.

The lift fluctuations increase again as the Reynolds number is increased in TrBL2 up to the beginning of the post-critical TrBL4 flow regime. This increase is steeper as the spacing ratio is larger, especially with regard to the fluctuating lift of the rear cylinder. The fluctuating lift coefficients seem to eventually converge and remain constant at the largest tested Reynolds numbers. The lift fluctuations on the front cylinder remain relatively small in comparison with the ones on the rear cylinder.

Fig. 9 shows the variation of the fluctuating lift coefficient c_l' with the spacing ratio L/D at the main flow regimes, i.e. the sub-critical (Re = 45k), the critical (Re = 79k) and the post-critical (Re = 395k) flow regimes. Note that the Reynolds number representing the critical regime corresponds to the one associated with the minimum drag coefficient of the front cylinder. The results from the work of Alam et al. (2003) performed in the sub-critical flow regime on smooth cylinders are added for comparison.

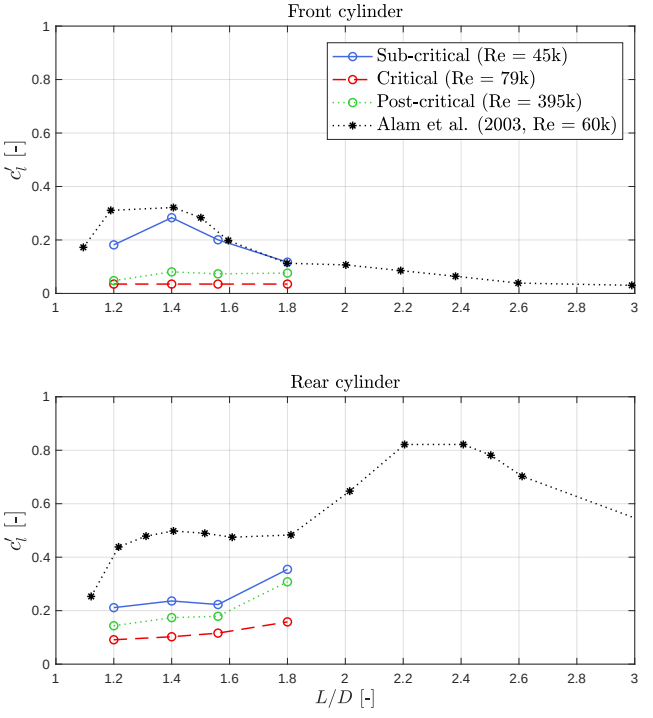

Figure 9: Variation of the fluctuating lift coefficient c_l' with the spacing ratio L/D at the three main flow regimes.

In the sub-critical flow regime, the fluctuating lift coefficients of both cylinders increase when the rear cylinder is moved downstream from L/D of 1.2 to 1.4. As the rear cylinder is moved further downstream, the fluctuations on the front cylinder decrease. On the other hand, the fluctuations on the rear cylinder first decrease when L/D is increased from 1.4 to 1.56 but increase again between 1.56 and 1.8. The same variations were measured by Alam et al. (2003),

as it can be seen in Fig. 9. They observed a local maximum of the fluctuating lift coefficients at a spacing ratio of 1.4. The values of the present study are though rather different in comparison with those obtained by Alam et al. (2003), especially for the rear cylinder. This discrepancy is incriminated to the difference of Reynolds number (Re = 45k versus 60k). Indeed, Zdravkovich (1997) showed for a single cylinder that the formation length of the eddies in the TrSL2 regime decreases with the Reynolds number. This decrease induces an increase of the fluctuating lift coefficient and a decrease of the Strouhal number. For tandem cylinders, it can be stated that it has a significant impact on the flow around rear cylinder.

In the critical flow regime, the fluctuating lift coefficient of the front cylinder does not vary with the spacing ratio. On the other hand, the fluctuations of the lift force acting on the rear cylinder increase with the spacing ratio.

Finally, in the post-critical flow regime, the fluctuating lift coefficient of the front cylinder remains rather small and constant, except between $L/D = 1.2$ and 1.4 where it slightly increases. The fluctuating lift coefficient of the rear cylinder increases with the spacing ratio and its values are a bit smaller than the ones obtained in the sub-critical flow regime.

3.3. Frequency content of the lift forces

The *Power Spectral Density* (*PSD*) of the fluctuating lift forces acting on the tandem cylinders is shown in Fig. 10 as a function of the Reynolds number. The temporal lift coefficients are initially normalized by their corresponding standard deviation. This procedure allows to compare the frequency content of the lift signal at each Reynolds number. Additionally, the frequency content of the lift force at particular Reynolds numbers are plotted in Fig. 11 in order to facilitate the observation of multiple peaks as discussed hereafter. It should be mentioned that the Reynolds numbers are chosen to illustrate the frequency contents at the main interesting flow regimes, i.e. the sub-critical (Re = 45k), the critical (Re = 74k and 79k: from one asymmetric flow to the other) and the post-critical (Re = 395k) flow regimes. The dimensionless Strouhal number $St = fD/U_\infty$ is used as the frequency variable. It varies in the range $0 \leq St \leq 0.75$ in the present analysis in order to include potential harmonics in the spectra.

For spacing ratios $L/D = 1.4$ to 1.8, a peak at very low-frequency ($St \approx 0.01$) is observed in the TrSL2 and beginning of TrBL0 regimes (Fig. 10(b-d)). It also clearly appears in Fig. 11(c-d) at Re = 45k. An interpretation of this peak is difficult because its corresponding frequency does not follow a common trend for the different spacing ratios: hence it cannot be attributed to a vortex shedding phenomenon. An attempt to explain this very low-frequency fluctuation is the meandering effect, similar to the one observed around the rotors of wind turbines. The following analyses focus on the higher frequency peaks associated to the vortex shedding phenomenon.

At the lowest Reynolds numbers, two peaks which do not correspond to harmonic frequencies can be observed in the spectra for spacing ratios $L/D \leq 1.4$ in Fig 10(a-b). This observation is made at Reynolds numbers Re < 36k and 28k for $L/D = 1.2$ and 1.4, respectively. Igarashi (1984) also observed two peaks in the frequency content of the fluctuating velocity behind the tandem arrangement for the same spacing ratios and Reynolds number ranges. Two peaks were identified in the Reynolds number ranges 19k ≤ Re ≤ 32k and 17k ≤ Re ≤ 25k for $L/D = 1.2$ and 1.4, respectively. He concluded that the occurrence of those two peaks is inferred to the intermittent re-attachment of the shear layers onto the rear cylinder. The same conclusion may therefore be stated in the present work. The peak at the largest Strouhal number ($St \approx 0.27$) corresponds to the extended-body regime, i.e. without re-attachment of the shear layers, and the other one ($0.15 \leq St \leq 0.2$) to the re-attachment regime. A single peak is observed for the two other spacing ratios (Fig. 10(c-d)) and it corresponds to the re-attachment regime as well. Its associated Strouhal number decreases with the Reynolds number in TrSL2 regime (see Fig. 10(a-d)).

When the Reynolds number increases, the peak at the largest Strouhal number ($St \approx 0.27$) disappears while the other one ($St \approx 0.15$) remains rather constant. A second peak appears at a harmonic frequency of the dominant peak. It is therefore assumed to emanate from the same physical phenomenon as the fundamental frequency and the flow pattern is not unstable anymore. This harmonic component is also present for spacing ratios $L/D = 1.56$ and 1.8 at the end of TrSL2 and TrBL0 regimes. The harmonic component clearly appears for each spacing ratio in Fig. 11 at Re = 45k (end of sub-critical regime). At this particular Re, a third peak can be observed at a higher harmonic frequency ($St \approx 0.4$) for $L/D = 1.2$ and 1.4 (Fig. 11(a-b)). Note that these third peaks do not appear in Fig. 10 because of their low energy level. In Fig. 11, one can see that the harmonic component decreases with the spacing ratio and even seems

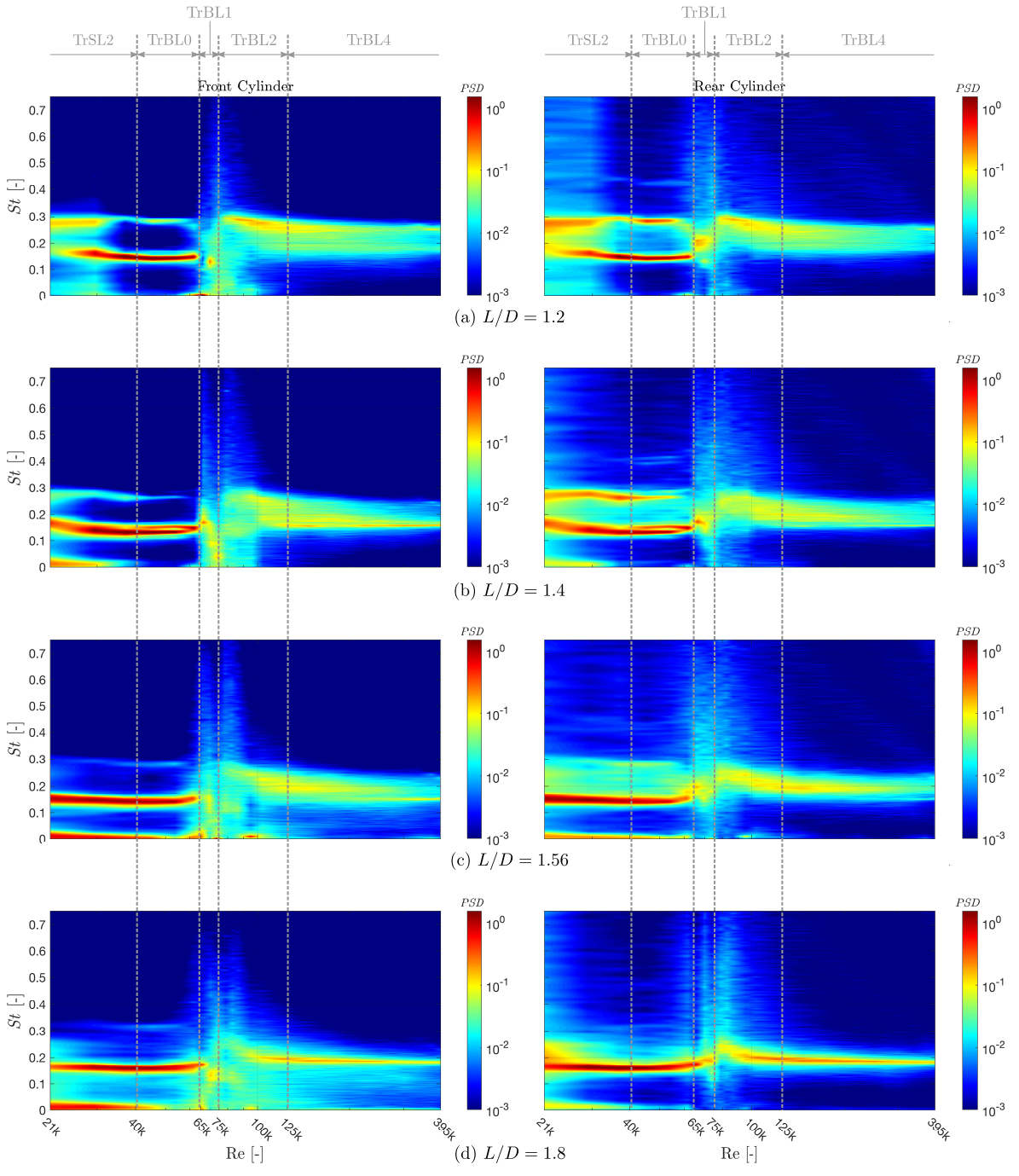

Figure 10: Variation of the frequency content of the lift force acting on the tandem cylinders with Re for the different spacing ratios L/D.

to disappear from the spectrum of the lift force of the rear cylinder for $L/D = 1.8$. "Double" peaks ($St \approx 0.15$ and 0.4) are observed for $L/D = 1.4$ in the TrBL0 regime (Figs. 10(b) and 11(b) at Re = 45k). Those peaks are due to a modulation of the temporal lift coefficient of each cylinder. Fig. 12 shows the temporal lift coefficients of the front and rear cylinders and the respective *PSD*s for the different spacing ratios at Re = 45k. The results obtained for the single cylinder at the same Re have been added for comparison. In this figure, the modulation of the lift signals for the spacing $L/D = 1.4$ is important and regular compared to the other spacing ratios. The "double" peaks detected in

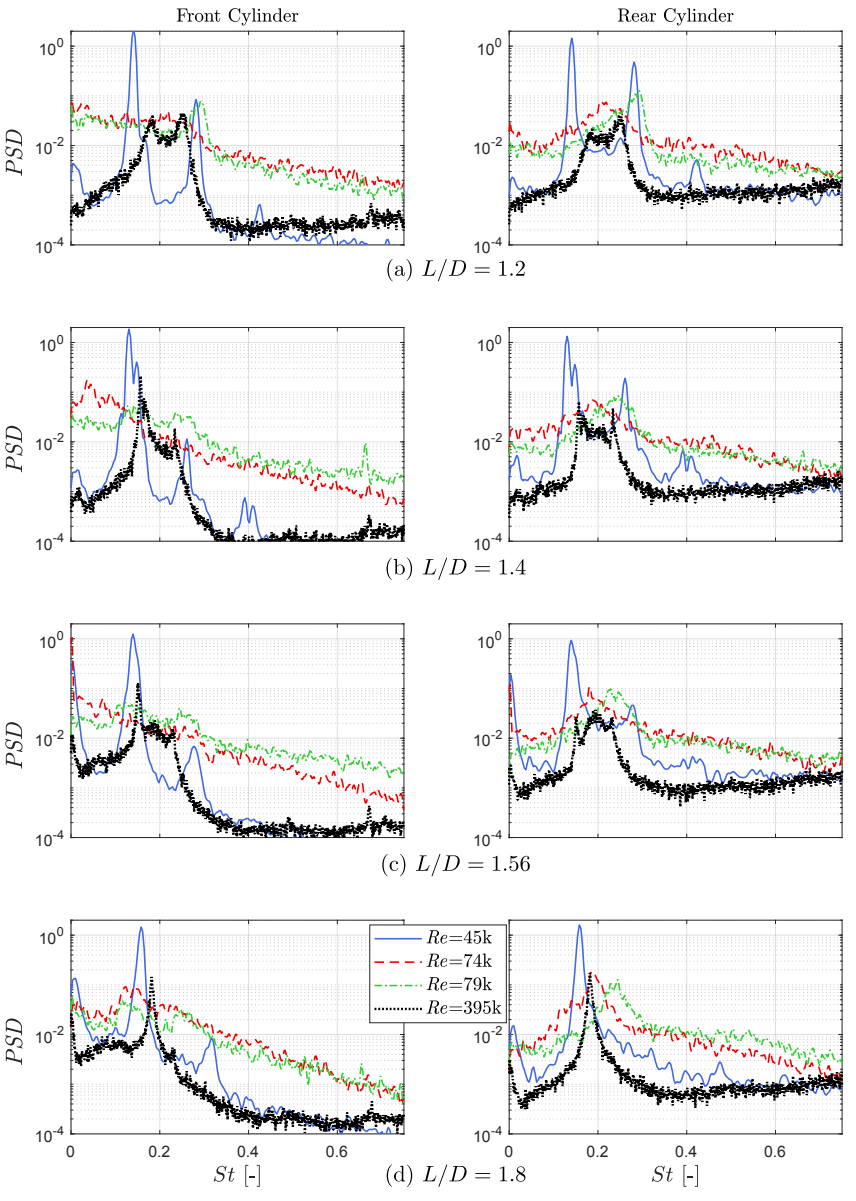

Figure 11: Frequency content of the lift force acting on the tandem cylinders at different Re for each spacing ratio L/D.

Fig. 11(b) are a consequence of this modulation and do not bring information on the physical phenomena taking place around the cylinders. Instead, they can be used to calculate the frequencies of two phenomena : (i) the vortex shedding taking place in the wake of the rear cylinder at $St = 0.13$ and (ii) a low frequency component at 0.39 Hz ($St \approx 0.009$) for which no physical explanation is found.

In the critical flow regime, the spectra become broadband and the peaks are flattened so that a clear single peak cannot be identified anymore for the front cylinder, as it can be seen in Fig. 11 at Re = 74k. The fluctuations of the lift coefficient of the front cylinder are thus considered as non-periodic and weakly impacted by the eddy shedding from the rear cylinder. A peak can still be identified for the rear cylinder for all spacing ratios. The associated Strouhal number increases with the Reynolds number in TrBL1 (see Fig. 10) and reaches a maximum value at the end of the critical regime. One can also notice the absence of a harmonic component in this regime. In TrBL2 regime, a peak slightly re-appears for the front cylinder at the same Strouhal number as for the rear cylinder, even though the spectra

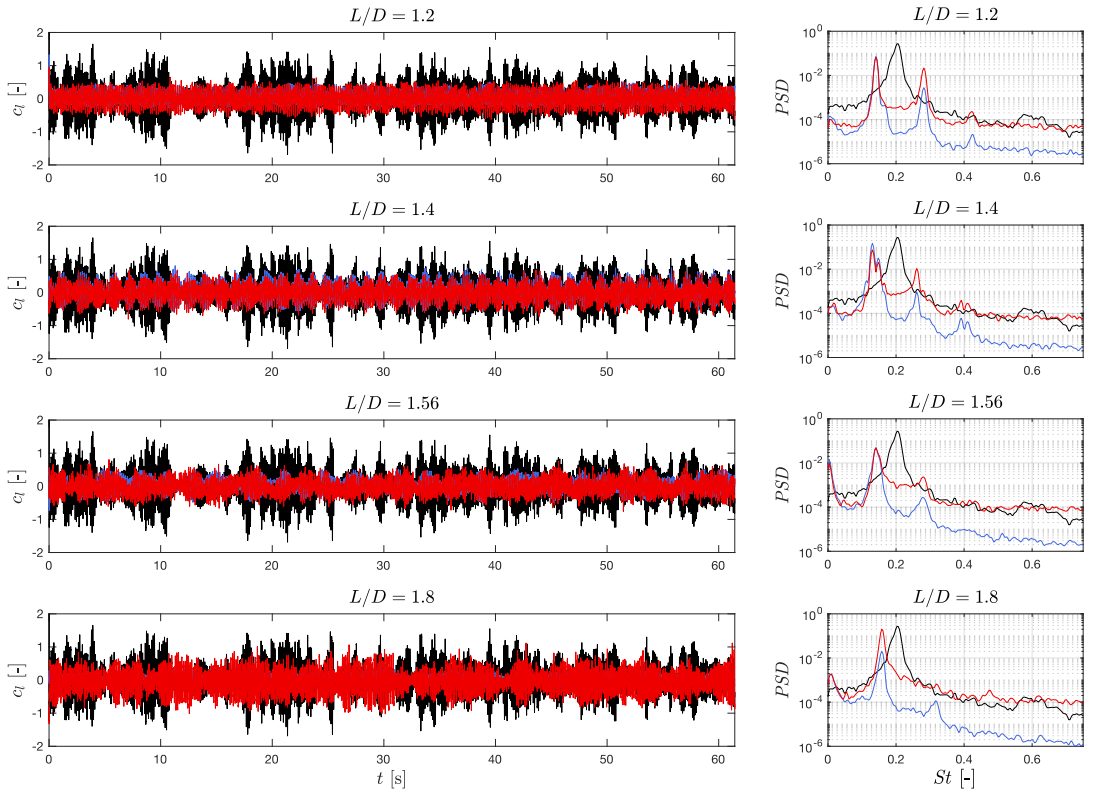

Figure 12: Temporal lift coefficients and respective *PSD*s of the single cylinder (black) and tandem cylinders (blue: front; red: rear) for the different spacing ratios at Re = 45k.

remain quite broadband. The Strouhal number decreases with the Reynolds number in TrBL2.

In the post-critical regime TrBL4, the spectra are sharper and peaks are easier to identify. At large Reynolds numbers, two peaks which do not correspond to harmonic frequencies are observed for spacing ratios $L/D \leq 1.56$. Those peaks clearly appear in Fig 11(a-c) at Re = 395k. This observation is similar to the one previously made at the lowest Reynolds numbers for spacing ratios $L/D \leq 1.4$. Therefore, an attempt to explain the occurrence of two peaks in the post-critical flow regime is the intermittent re-attachment of the separated shear layers from the front cylinder onto the rear cylinder. For $L/D = 1.8$, the spectra present a single peak (see Fig. 11(d)). It reflects the stable behaviour of the shear layers for this configuration: they do not re-attach intermittently anymore.

Based on the previous observations and discussions, it can be stated that the eddy shedding phenomenon, which is the most energetic one, is identified in the range $0.13 < St < 0.32$ (by including the first harmonic components) depending on the Reynolds number and spacing ratio.

Fig. 13 shows the Strouhal number associated to the eddy shedding as a function of the spacing ratio L/D at the three main flow regimes. Literature results for tandem cylinders are added for comparison. Additionally, the dashed-dotted lines correspond to the Strouhal numbers of a single rough cylinder. It should be mentioned that the results from Igarashi (1981) and Alam et al. (2003) correspond to smooth cylinders while the ones from Okajima (1979) correspond to rough cylinders ($k/D = 9 \times 10^{-3}$).

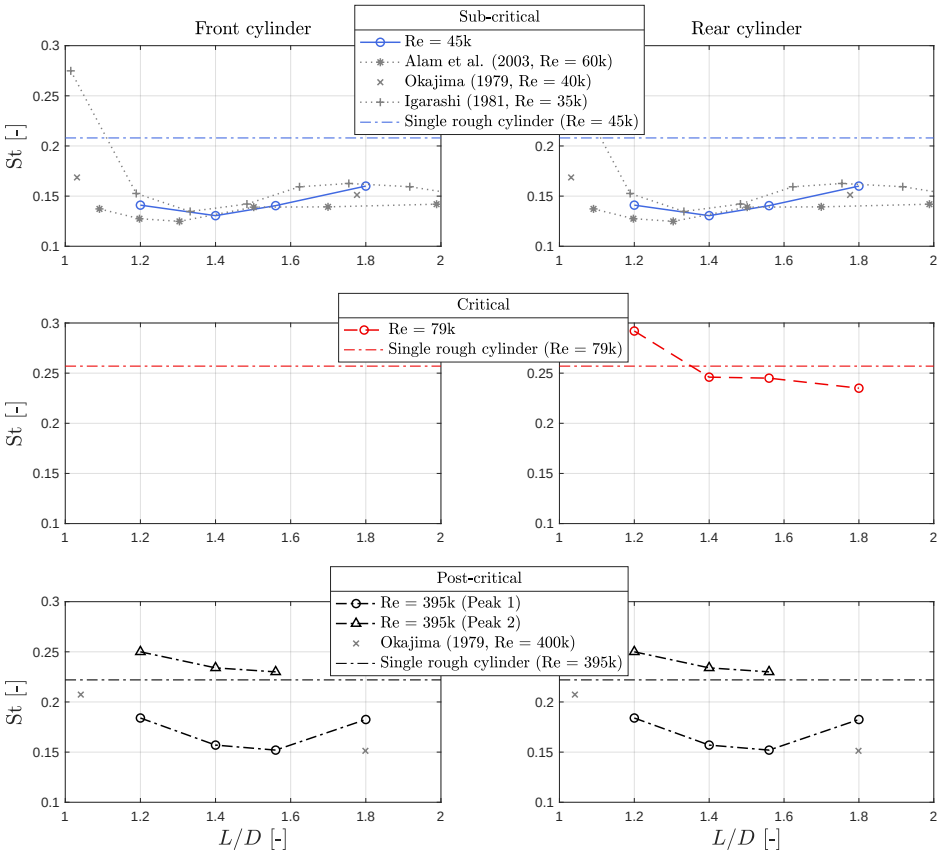

Figure 13: Variation of the Strouhal number with the spacing ratio L/D at the three main flow regimes.

In the sub-critical flow regime, the Strouhal number decreases from 0.141 to 0.13 between $L/D = 1.2$ and 1.4. When the spacing ratio between the cylinder is further increased, the Strouhal number increases up to 0.16 for $L/D = 1.8$. Alam et al. (2003) and Igarashi (1981) observed the same trend for the Strouhal number with the spacing ratio in the sub-critical regime, with a local minimum value in the range $1.3 < L/D < 1.4$. The values of the Strouhal number measured by Alam et al. (2003) are nevertheless slightly smaller. It is incriminated to the difference of Reynolds number, as already explained in the previous section. Okajima (1979) performed only two experiments within the spacing ratio range of interest ($1 < L/D < 2$). It is therefore difficult to compare the evolution of the Strouhal number in this range. The quantitative values are though in good agreement with the other experiments.

In the critical flow regime, one can see that Strouhal numbers are shown only for the rear cylinder. It is justified by the broadband frequency content of the fluctuating lift force acting on the front cylinder which flattens the peaks and makes their identification approximate. As it was stated earlier, the fluctuations on the front cylinder are mostly non-periodic. That being said, the Strouhal number of the rear cylinder monotonically decreases with the spacing ratio. It is also interesting to note that the Strouhal number is larger than the one of a single cylinder when $L/D = 1.2$ and becomes smaller for the other spacing ratios. To the authors' knowledge, no literature results in this particular regime could be found for comparison.

In the post-critical flow regime, one can identify two Strouhal numbers for $L/D \leq 1.56$ in Fig. 13, corresponding to the two peaks observed in Figs. 10 and 11. The largest Strouhal number (i.e. peak 2 in Fig. 13) decreases with the spacing ratio and seems to converge towards the value obtained from a single cylinder. The other Strouhal number decreases from 0.184 to 0.152 between $L/D = 1.2$ and 1.56 and increases to 0.183 when the spacing ratio is increased

to $L/D = 1.8$. This latter evolution is quite similar to the one observed in the sub-critical flow regime, although the spacing ratio at which the minimum value of the Strouhal number occurs is not the same and the values are larger in the post- than in the sub-critical regime. Okajima (1979) reported only one peak and hence a unique Strouhal number. As stated in the sub-critical regime, he performed only two experiments within the spacing ratio range of interest. It is thus difficult to compare the evolution of the Strouhal number with his results. For $L/D = 1.8$, the value of the Strouhal number measured by Okajima (1979) is around 0.15 and it is equal to 0.183 in the present work, even though the Reynolds number and the relative surface roughness are equivalent. The only difference between the two works is the technique used to extract the Strouhal number: Okajima (1979) computed it from the fluctuating velocity in the wake while it is computed from the fluctuating lift in the present investigation.

3.4. Pressure distributions

The pressure distributions measured around the tandem cylinders are presented for each spacing ratio L/D at three different Reynolds numbers representing the main flow regimes.

The time-averaged pressure coefficient distributions at the three different flow regimes are plotted in polar coordinates for $L/D = 1.2$ in Fig. 14(a). The distributions are nearly symmetric with respect to the centreline between the cylinders at Re = 45k and 395k, i.e. in the sub- and post-critical regimes. A negligible asymmetry is observed and most likely emanates from a slight misalignment of the set-up regarding the incoming flow, as it was already mentioned when analysing the time-averaged lift coefficients. At the end of the critical flow regime (Re = 79k), the pressure distribution of each cylinder is strongly asymmetric. These observations are in agreement with the ones of the time-averaged lift coefficients of both individual cylinders: the lift coefficients are found to be nearly zero in TrSL2, TrBL0 and TrBL4 regimes while they are clearly non-zero in TrBL1 and TrBL2 (Fig. 7). The pressure distributions around the front cylinder are similar to the ones observed around a single cylinder. The pressure distributions around the rear cylinder present two local maximum values on its forward face at angular positions which depend on the Reynolds number. It is inferred that these angular locations correspond to the time-averaged re-attachment points of the separated shear layers from the front cylinder, as observed by Igarashi (1981) and Alam et al. (2003). Even though they do not clearly appear in Fig. 14(a), small local maximum values are also found at the back of the front cylinder. This observation reveals the re-attachment of shear layers emanating from the forward face of the rear cylinder onto the front cylinder.

The fluctuating pressure coefficient distributions for $L/D = 1.2$ are shown in polar coordinates in Fig. 14(b). Similarly to the time-averaged distributions, they are nearly symmetric at Re = 45k and 395k and clearly asymmetric at Re = 79k. Concerning the front cylinder, maximum fluctuating pressure coefficients are located between $\pm 65°$ and $\pm 110°$, depending on the Reynolds number. These maximum values are caused by the separation of the boundary layers. Local maximum values are also observed at the back of the front cylinder at $\theta \approx \pm 150°$ in the sub- and post-critical regimes (Re = 45k and 395k) and $\theta \approx 180°$ in the critical regime (Re = 79k). As stated above, those are inferred to the re-attachment of the shear layers emanating from the forward face of the rear cylinder onto the front cylinder. Concerning the rear cylinder, the maximum fluctuating pressure coefficients are located around the re-attachment points of the shear layers from the front cylinder. At Re = 45k, for example, the re-attachment points are located at the angular positions $\theta \approx \pm 75°$ and the maximum fluctuating pressure coefficients at $\theta \approx \pm 70°$. This observation reports the important effect of the buffeting of the shear layers on the pressure fluctuations acting on the rear cylinder. The other local maximum values observed in the distributions around the rear cylinder are linked to the separation of the boundary layers.

Figs. 14(c)-(e) show the spectra of the fluctuating pressure coefficients around the cylinders for $L/D = 1.2$ at the three different Reynolds numbers. The radial direction corresponds to the frequency variable, represented by the dimensionless Strouhal number, and the tangential direction refers to the angular location around the cylinders. Similarly to the previous quantities, the spectra are nearly symmetric with respect to the centreline between the cylinders in the sub- and post-critical regimes. The spectra in the critical regime are also clearly asymmetric. In the sub-critical flow regime (Re = 45k), a dominant frequency is observed at $St = 0.141$ for each cylinder and its harmonic component ($St = 0.282$) is also observable in the spectra. An interesting observation concerns the broadband frequency content of the fluctuations at an energy level around 10^{-3} Hz^{-1} near the re-attachment points on the rear cylinder and slightly smaller near the ones on the back face of the front cylinder. This broadband energy distribution is characteristic of turbulent shear layers. This observation is also valid for the two other flow regimes (Fig. 14(d)-(e)). In the critical flow regime, a peak is found at $St = 0.292$ but its energy level is rather small in comparison with the sub-critical regime.

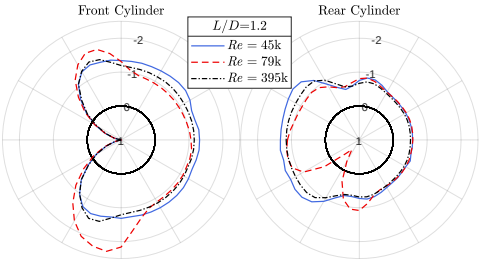

(a) Time-averaged pressure coefficient C_p distribution

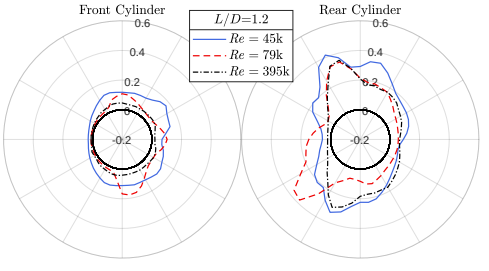

(b) Fluctuating pressure coefficient C'_p distribution

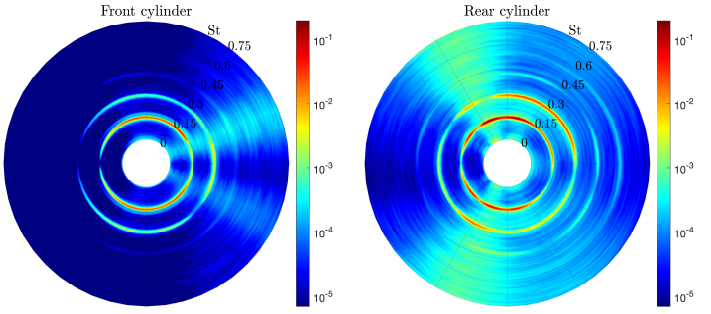

(c) *PSD* of the temporal pressure coefficients at Re = 45k

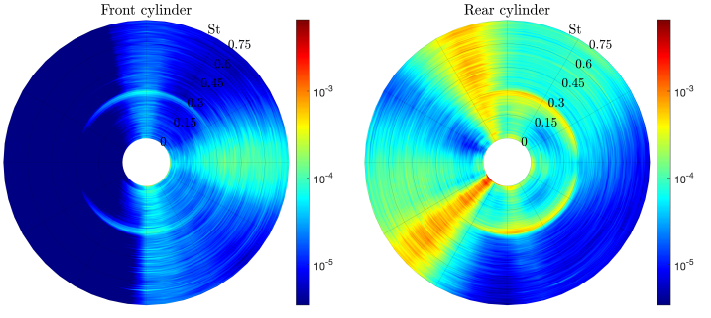

(d) *PSD* of the temporal pressure coefficients at Re = 79k

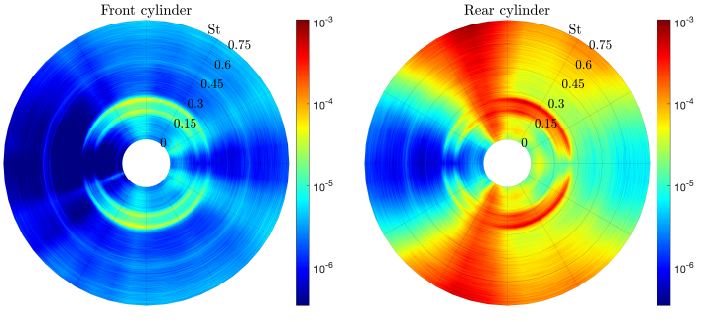

(e) *PSD* of the temporal pressure coefficients at Re = 395k

Figure 14: Pressure coefficient around the tandem cylinders for $L/D = 1.2$ in the main flow regimes.

Indeed, it is balanced by the the broadband frequency contents near the re-attachment points. In the post-critical flow regime, two peaks can be identified in the spectra. One can notice that the second peak ($St = 0.25$) do not appear at a harmonic frequency of the first peak ($St = 0.184$). The occurrence of those two Strouhal numbers was previously observed in the frequency content of the fluctuating lift coefficients at the same Reynolds number (see Fig. 11(a)). It is attributed to the intermittent re-attachment of the separated shear layers from the front cylinder onto the rear cylinder. This intermittent behaviour of the shear layers may explain the low energy level associated to the identified peaks in the spectra (Fig. 14(e)).

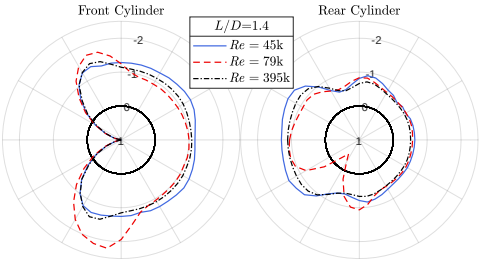

(a) Time-averaged pressure coefficient C_p distribution

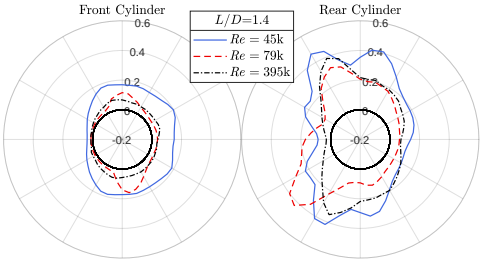

(b) Fluctuating pressure coefficient C_p' distribution

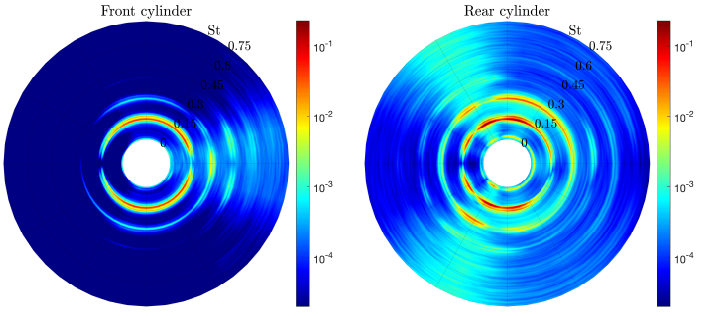

(c) *PSD* of the temporal pressure coefficients at Re = 45k

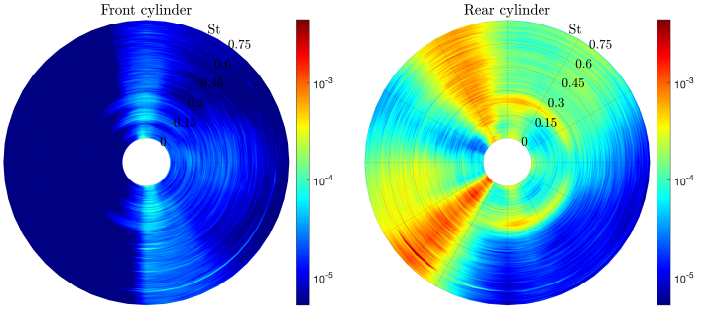

(d) *PSD* of the temporal pressure coefficients at Re = 79k

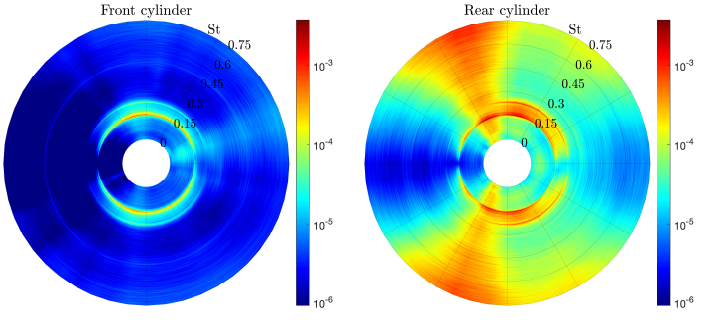

(e) *PSD* of the temporal pressure coefficients at Re = 395k

Figure 15: Pressure coefficient around the tandem cylinders for $L/D = 1.4$ in the main flow regimes.

The different quantities of the pressure coefficients around tandem cylinders spaced by $L/D = 1.4$ are shown in Fig. 15. The same general observations can be made on the time-averaged and fluctuating pressure coefficient distributions in comparison with the previous spacing ratio. As a matter of fact, the distributions of the different quantities are nearly symmetric in the sub- and post-critical regimes and highly asymmetric in the critical regime with respect to the centreline between the cylinders. Local maximum values in the time-averaged pressure distributions on the forward face of the rear cylinder and on the back face of the front cylinder are observed, reporting the occurrence of the re-attachment of shear layers. In the sub-critical flow regime, a dominant peak in the frequency content of the fluctuating pressure coefficients on both cylinders is found at $St = 0.13$ (see Fig. 15(c)). One can notice that its first harmonic also contributes to the fluctuations, similarly to the previous spacing ratio. In the critical flow regime, the

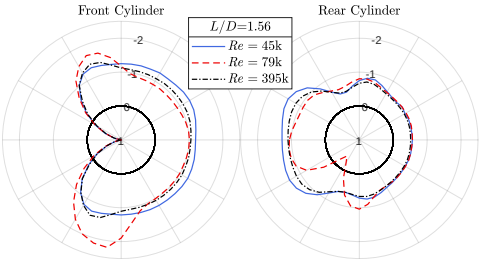

(a) Time-averaged pressure coefficient C_p distribution

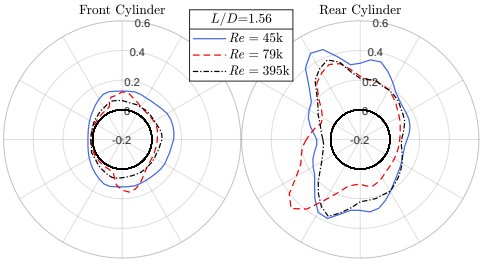

(b) Fluctuating pressure coefficient C_p' distribution

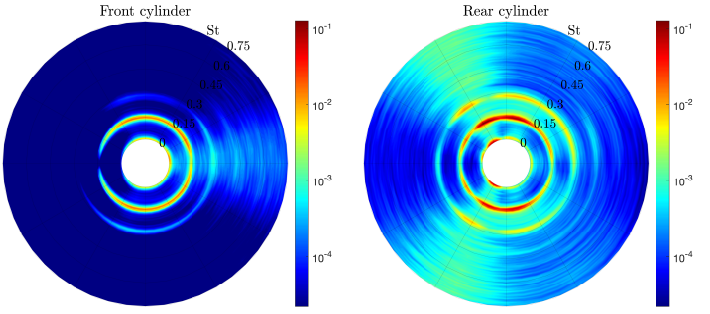

(c) *PSD* of the temporal pressure coefficients at Re = 45k

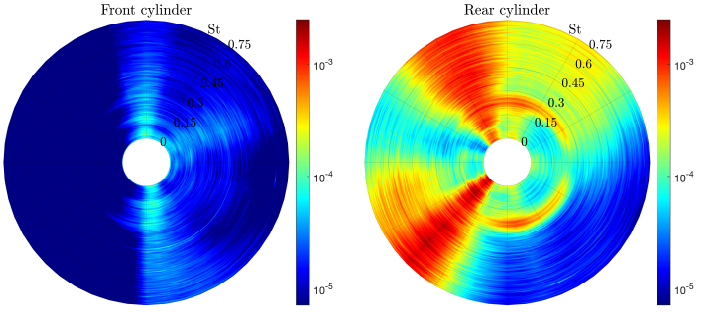

(d) *PSD* of the temporal pressure coefficients at Re = 79k

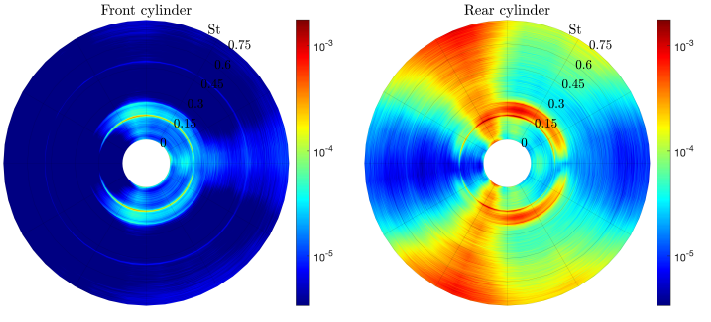

(e) *PSD* of the temporal pressure coefficients at Re = 395k

Figure 16: Pressure coefficient around the tandem cylinders for $L/D = 1.56$ in the main flow regimes.

spectra are quite broadband but a small peak can be observed at $St = 0.245$ at the back of the rear cylinder. However, unlike for the previous spacing ratio (Fig. 14(d)), a clear peak is not observed in the spectra around the front cylinder. In the post-critical regime, two peaks are observed at non-harmonic frequencies, similarly to the previous spacing ratio. Once again, it is attributed to the intermittent re-attachment of the shear layers. It is noticed that the peak at $St = 0.16$ is larger compared to the one at $St = 0.23$. Moreover, the largest energy levels of the second identified peak ($St = 0.23$) are mainly found at the back of the rear cylinder while they are located near and on each side of the re-attachment points on the rear cylinder for the first peak ($St = 0.16$). This observation supports the affirmation that the peak associated to $St = 0.23$ corresponds to the extended-body pattern (no re-attachment) and the one associated to $St = 0.16$ to the re-attachment pattern which will be discussed in the next section.

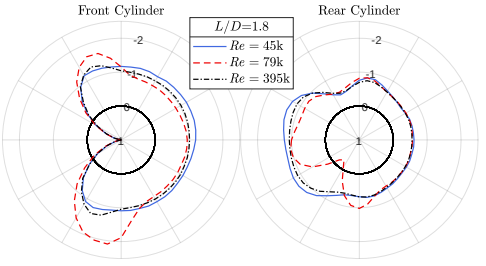

(a) Time-averaged pressure coefficient C_p distribution

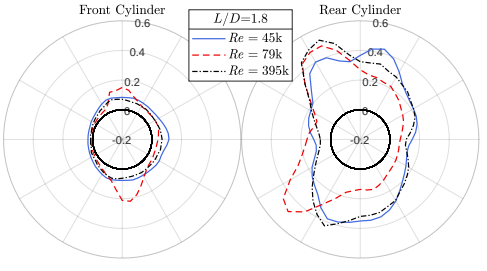

(b) Fluctuating pressure coefficient C'_p distribution

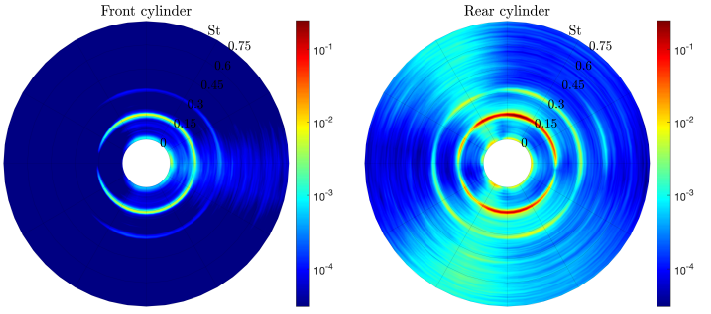

(c) *PSD* of the temporal pressure coefficients at Re = 45k

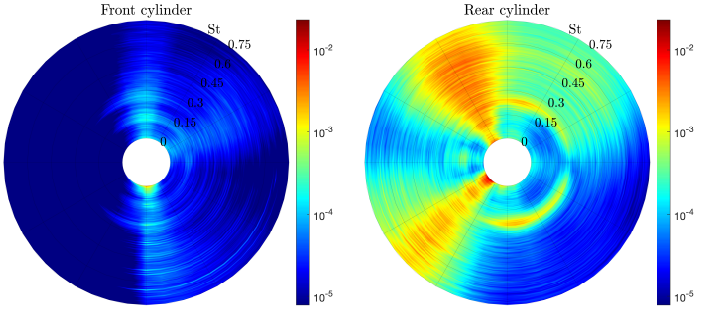

(d) *PSD* of the temporal pressure coefficients at Re = 79k

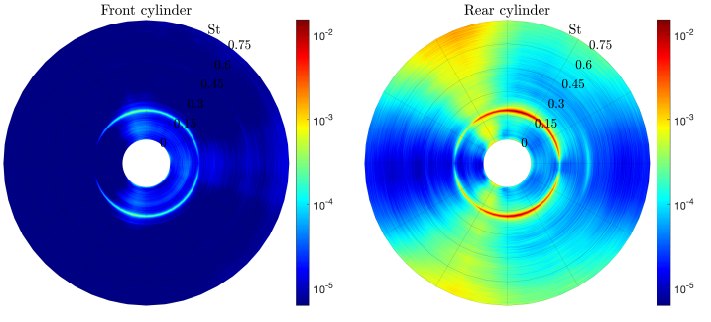

(e) *PSD* of the temporal pressure coefficients at Re = 395k

Figure 17: Pressure coefficient around the tandem cylinders for $L/D = 1.8$ in the main flow regimes.

The different quantities of the pressure coefficients around tandem cylinders spaced by $L/D = 1.56$ are shown in Fig. 16. Similarly to the previous spacing ratios, one can observe that the distributions of the different quantities are symmetric in the sub- and post-critical regimes and highly asymmetric in the critical regime. The occurrence of the re-attachment of the shear layers onto the rear cylinder is also inferred by the presence of local maximum values in the time-averaged pressure distributions on its forward face. In the sub-critical flow regime, the dominant peak is found at $St = 0.14$ in the spectra. Once again, a harmonic component to the pressure fluctuations is observed. In the critical flow regime, the observations about the spectra are the same as for the previous spacings. In the post-critical flow regime, two peaks at non-harmonic frequencies are again observed in the spectra. The fluctuations on the front cylinder are mainly dominated by the Strouhal number $St = 0.15$. The frequency content is more broadband on the

rear cylinder. However, one can identify the second peak at $St = 0.23$ at the back of the same cylinder. The spectra near and on each side of the re-attachment points of the shear layers onto the rear cylinder present a dominant peak a $St = 0.15$ like for the front cylinder. This is in agreement with the observation and affirmation made for the previous spacing ratio.

The different quantities of the pressure coefficients around tandem cylinders spaced by $L/D = 1.8$ are shown in Fig. 17. Again, the distributions of the different quantities are symmetric in the sub- and post-critical regimes and highly asymmetric in the critical regime. The location of re-attachment points of the shear layers onto the rear cylinder are identified from the observation of local maximum values in the time-averaged pressure distributions. In the sub-critical flow regime, a peak is found in the spectra at $St = 0.16$, together with its harmonic, similarly to the previous spacing ratios. The main difference with the previous spacing ratios is the observation of a single peak at $St = 0.18$ in the spectra of the fluctuating pressure coefficients in the post-critical regime (Fig. 17(e)). Multiple peaks are not observed and it is concluded that the re-attachment of the shear layers onto the rear cylinders is not intermittent anymore. Note also that a harmonic component is not observed as in the sub-critical flow regime.

As a summary, Table 3 gathers the numerical values of the time-averaged separation and re-attachment points on the two cylinders for the different spacing ratios in the main flow regimes. They are estimated from the time-averaged pressure distributions and spectra. The different points are defined in Fig. 18. The approximate separation angles are defined as suggested by Niemann (1971) and are obtained with a maximum angular resolution of 7.5°, i.e. the minimum angular distance between subsequent pressure taps.

Table 3
Time-averaged separation and re-attachment points on the two cylinders for the different spacing ratios and at the three main flow regimes (NR: No Re-attachment of the shear layer from the rear cylinder onto the back of the front one).

Regimes	L/D	θ_{SL1} [°]	θ_{SU1} [°]	θ_{SL2} [°]	θ_{SU2} [°]	θ_{RL1} [°]	θ_{RU1} [°]	θ_{RL2} [°]	θ_{RU2} [°]	θ_{FSL} [°]	θ_{FSU} [°]
sub-critical	1.2	75	-75	120	-120	157.5	-160	78	-75	30	-22.5
	1.4	75	-75	120	-120	160	-160	72.5	-70	15	-15
	1.56	75	-75	120	-120	NR	NR	75	-72.5	7.5	-7.5
	1.8	75	-75	120	-120	NR	NR	80	-70	7.5	0
critical	1.2	105	-97.5	112.5	-120	180	-180	50	-75	-15	-37.5
	1.4	105	-97.5	112.5	-120	180	-180	52.5	-68	-22.5	-30
	1.56	105	-97.5	112.5	-120	NR	-160	52.5	-68	-22.5	-30
	1.8	105	-97.2	112.5	-120	NR	-150	50	-65	-15	-22.5
post-critical	1.2	90	-90	120	-120	157.5	-157.5	80	-80	30	30
	1.4	90	-90	120	-120	160	-160	77.5	-75	22.5	-22.5
	1.56	90	-90	120	-120	NR	NR	75	-72.5	15	-7.5
	1.8	90	-90	120	-120	NR	NR	75	-70	15	-15

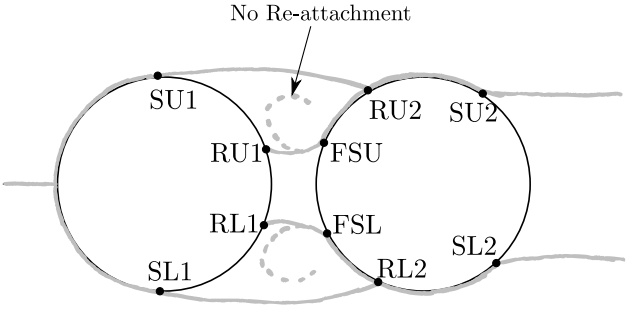

Figure 18: Definition of the separation and re-attachment points on the tandem cylinders (S: Separation; FS: Forward Separation; R: Re-attachment / U: Upper; L: Lower).

4. Discussion

Fig. 19 shows the different flow patterns around the tandem cylinders that can be observed within the tested Reynolds number and spacing ratio ranges. The grey sketches show the time-averaged flows while the black curves represent the instantaneous ones. The position of the shear layers are inspired by the work of Alam et al. (2003) and Igarashi (1981). In that sense, the sketches are intended to facilitate the discussion about the flows for different configurations.

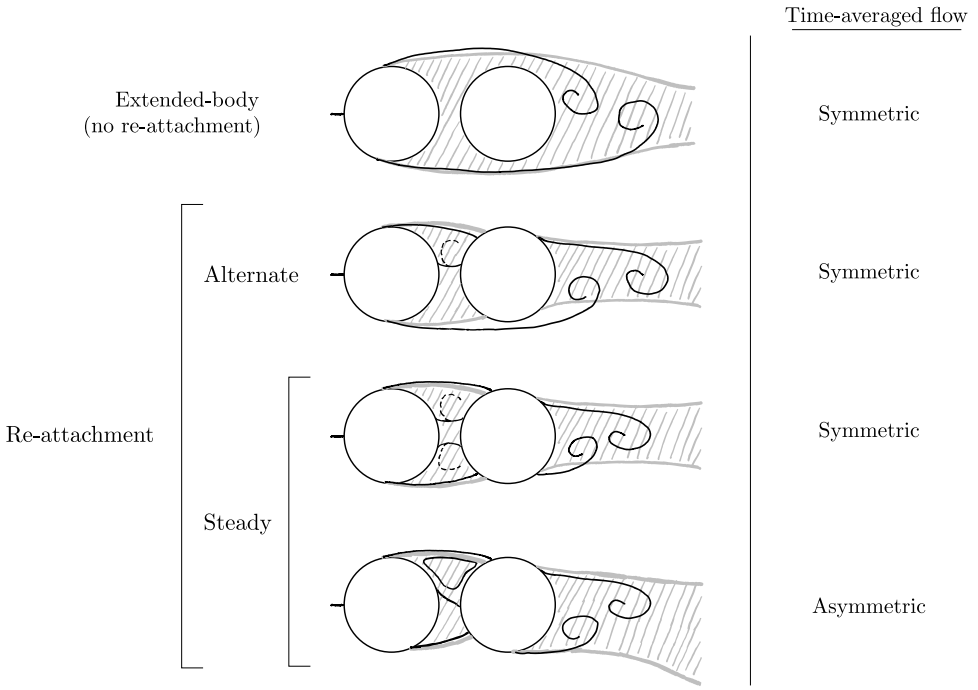

Figure 19: Sketches of the different flow patterns around tandem cylinders: time-averaged flow (in grey), instantaneous flow/shear layers (in black).

The first pattern is called the extended-body pattern. The separated shear layers from the front cylinder do not re-attach onto the rear cylinder and they alternately roll up and form eddies in the near wake of the rear cylinder. The time-averaged flow of the extended-body pattern is symmetric, as represented in the top sketch of Fig. 19. This pattern corresponds to the Pattern A identified by Igarashi (1981).

The three other patterns belong to the re-attachment regime: (i) the alternate and (ii-iii) steady re-attachment patterns. For the alternate re-attachment pattern, the separated shear layers from the front cylinder re-attach alternately: the separated shear layer on one side re-attaches on the rear cylinder while the shear layer on the other side does not and rolls up behind the rear cylinder to form an eddy. Half a period later, the situation is the opposite. As for the previous pattern, the time-averaged flow is symmetric. This pattern corresponds to the Pattern B identified by Igarashi (1981). For the steady re-attachment patterns, although the separated shear layers do fluctuate, they always re-attach onto the rear cylinder, as shown by the black curves in the two lower sketches of Fig. 19. Eddies are shed behind the rear cylinder. Two different time-averaged flows can be identified for this specific behaviour of the separated shear layers: one symmetric and the other one asymmetric. The pattern corresponding to the symmetric time-averaged flow is Pattern C identified by Igarashi (1981). Note that when a separated shear layer re-attaches onto the rear cylinder, it splits into two boundary layers: (i) one flowing in the downstream direction and (ii) the other one in the upstream direction. The former separates at the back of the rear cylinder while the latter separates at its front. This forward

separation leads to a separated shear layer going upstream which can either re-attach on the back surface of the front cylinder or roll up between the cylinder, depending on the spacing ratio L/D. Those flow patterns are sketched in Fig 19, with dotted black lines corresponding to the case of no re-attachment onto the back of the front cylinder.

Fig. 20 shows the identified flow patterns around the tandem cylinders for each spacing ratio at three Reynolds numbers. The Reynolds numbers were chosen to represent the main flow regimes. The flow patterns are identified based on the quantitative analyses presented in the previous sections.

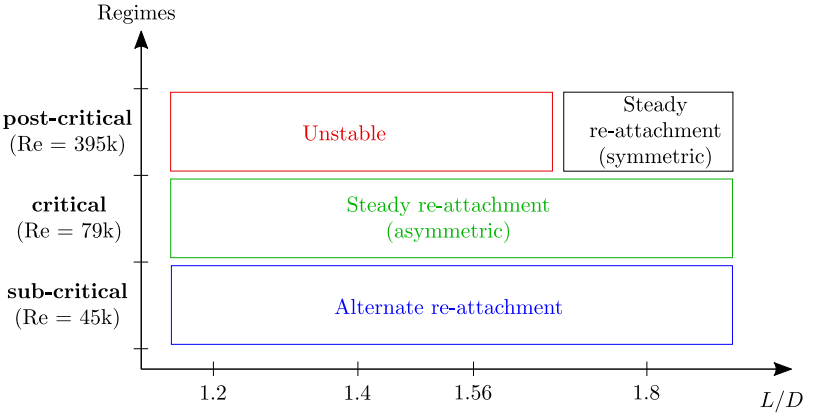

Figure 20: Identified flow patterns for each spacing ratio at the main flow regimes

In the sub-critical regime (Re = 45k), the mean flow is symmetric with respect to the centreline between the cylinders. The symmetry can be visualised in the time-averaged pressure distributions (Figs. 14-17(a)) and lift forces (Fig. 7). For each spacing ratio, the flow pattern corresponds to an alternate re-attachment of the separated shear layers from the front cylinder onto the rear cylinder. This particular flow pattern is inferred by the presence of harmonic frequencies in the spectra (see Figs. 14-17(c)). The latter association of the occurrence of alternate re-attachment with the presence of harmonic frequencies in the spectra of the pressure distribution was proposed by Alam et al. (2003).

In the critical regime, the symmetry of the mean flow is lost. The separation points on the front cylinder are not located at the same stream-wise positions. It leads to the asymmetry of the pressure distributions (Figs. 14-17(a)) and non-zero lift forces acting on the cylinders (Fig. 7). In this regime, the resulting flows are characterised by a steady re-attachment: upper and lower shear layers fluctuate but always re-attach on the rear cylinder. As a matter of fact, no harmonic frequency can be observed in the frequency content of the pressure fields around the two cylinders. Moreover, the re-attachment points do not fluctuate at a single frequency. Instead, the frequency contents near the re-attachment points are broadband which is characteristic of non-periodic fluctuations (see Figs. 14-17(d)). The eddy shedding still occurs behind the rear cylinder in the critical regime. It is confirmed by the presence of a peak in the spectra of the fluctuating pressure at the back of the rear cylinder (see Figs. 14-17(d)). Nonetheless, the energy of the corresponding peak is balanced by the region of re-attachment which is characterised by a broadband frequency content. Hence, the effect of the eddy shedding on the flow is significantly reduced compared to the sub-critical regime. This observation is in agreement with the drop of c_l' of both cylinders reported in the critical flow regime (see Fig. 8). That being said, one can state that the flow pattern for each spacing ratio is the steady re-attachment one with the asymmetric time-averaged flow shown in Fig. 19.

In the post-critical flow regime, the mean flow retrieves its symmetry: the pressure distributions are symmetric with respect to the centreline between the cylinders (Figs. 14-17(a)) and the resulting lift forces are equal to zero (Fig. 7). For the first three spacing ratios ($L/D \leq 1.56$), multiple peaks are present in the spectra of the lift coefficients which do not appear at harmonic frequencies (see Fig. 11). This observation is discussed in section 3.1.3 and an attempt to explain the occurrence of the two peaks is the intermittent re-attachment of the separated shear layers from the front cylinder onto the rear cylinder. This leads to an unstable pattern which intermittently fluctuates between the extended-

body pattern and the steady re-attachment pattern shown in Fig. 19. For the spacing ratio $L/D = 1.8$, a single peak is observed in the frequency content. The corresponding flow pattern is characterised by a steady re-attachment. It is corroborated by the absence of harmonic frequencies of the Strouhal number associated to the peak in the spectra (see Figs. 17(e)).

5. Conclusions

The flow around static tandem cylinders is investigated from sub- to post-critical regimes. The critical regime is reached around Re = 60k by using a surface roughness characterised by a relative height equal to $k/D = 7.2 \times 10^{-3}$. A special attention is given to the span-wise roughness of the cylinders. The tandem rough cylinders are investigated for different spacing ratios ($L/D = 1.2$, 1.4, 1.56 and 1.8) in low turbulence flow conditions.

The following conclusions are drawn:

- The variation of the time-averaged lift and drag coefficients with the Reynolds number is used to identify the flow regimes around the tandem cylinders. The identification follows the classification proposed by Zdravkovich (1997) for a single cylinder.
- A comparison of the drag coefficients of smooth and rough cylinders shows that the surface roughness has a significant effect on the flow around the tandem arrangement in the different flow regimes, especially in the critical regime.
- For the front cylinder and all spacings, the fluctuating component of the lift coefficient is lower than the one corresponding to a single cylinder for all flow regimes.
- This conclusion holds for the rear cylinder in the sub-critical flow regime only.
- In the post-critical regime, the lift fluctuations acting on the rear cylinder increase as the spacing increases. They are always larger than the corresponding value for the single cylinder.
- Eddy shedding phenomenon is identified in the range $0.13 < St < 0.32$ (including first harmonic component) depending on the Reynolds number and spacing ratio.
- The frequency content of the lift force shows a sharp peak and its harmonic in the sub-critical flow regime. In the critical and post-critical regimes, the gap flow is more stable and the effect of the eddy shedding on the front cylinder is less severe. The eddy shedding is still present on the rear cylinder.
- In the post-critical flow regime, two peaks at non-harmonic frequencies are observed in the spectra of the lift forces for $L/D \leq 1.56$. It is explained by the intermittent re-attachment of the separated shear layers from the front cylinder onto the rear cylinder.
- For $L/D = 1.8$, a single peak is observed in the spectra of the lift forces. It is concluded that the behaviour of the shear layers is stable and they re-attach onto the rear cylinder.

These findings are summarised in a discussion about the flow around the tandem cylinders. The features of the shear layers are analysed for the different regimes and spacing ratios. It is concluded that the flow belongs to the re-attachment pattern for all spacing ratios in the sub- and critical regimes. In accordance with the work of Alam et al. (2003), the re-attachment is alternate in the sub-critical regime. The re-attachment becomes steady with an asymmetric time-averaged flow in the critical regime. In the post-critical flow regime, the flow pattern is unstable for $L/D \leq 1.56$: it intermittently fluctuates between the extended-body and steady re-attachment patterns. For $L/D = 1.8$, the shear layers steadily re-attach onto the rear cylinder and the flow belongs to the steady re-attachment pattern. Note that all experimental results and conclusions about the different phenomena reported in this study are limited to the tested roughness levels and Reynolds numbers ranges. If scaling is planned based on the present results, the reader should take care of the similarities regarding the Reynolds number and the roughness parameter k/D. Indeed, comparing the present results with the ones from Schewe and Jacobs (2019), it is stated that the flow (hence aerodynamic quantities) is not the same for smooth or rough cylinders at different Reynolds number although it is in the same flow regime.

References

Achenbach, E., 1971. Influence of surface roughness on the cross-flow around a circular cylinder. Journal of Fluid Mechanics 46, 321–335. doi:https://doi.org/10.1017/S0022112071000569.

Adachi, T., 1997. Effects of surface roughness on the universal strouhal number over the wide reynolds number range. Journal of Wind Engineering and Industrial Aerodynamics 69, 399–412. doi:https://doi.org/10.1016/S0167-6105(97)00172-4.

Alam, M.M., Moriya, M., Takai, K., Sakamoto, H., 2003. Fluctuating fluid forces acting on two circular cylinders in a tandem arrangement at a subcritical reynolds number. Journal of Wind Engineering and Industrial Aerodynamics 91, 139–154. doi:https://doi.org/10.1016/S0167-6105(02)00341-0.

Bearman, P.W., Wadcock, A.J., 1973. The interaction between a pair of circular cylinders normal to a stream. Journal of Fluid Mechanics 61, 499–511. doi:10.1017/S0022112073000832.

Bergh, H., Tijdeman, H., 1965. Theoretical and experimental results for the dynamic response of pressure measurement systems. National Aero-and Astronautical Research Institute (Netherlands), Report NLR-TR F 238.

Biermann, D., Herrnstein, W., 1933. The interference between struts in various combinations. National Advisory Committee for Aeronautics. Technical Report. Tech. Rep. 468.

Fage, A., Warsap, J., 1929. The effects of turbulence and surface roughness on the drag of a circular cylinder. r. &m. no. 1283. British ARC .

Güven, O., Farell, C., Patel, V., 1980. Surface-roughness effects on the mean flow past circular cylinders. Journal of Fluid Mechanics 98, 673–701. doi:https://doi.org/10.1017/S0022112080000341.

van Hinsberg, N.P., 2015. The reynolds number dependency of the steady and unsteady loading on a slightly rough circular cylinder: From subcritical up to high transcritical flow state. Journal of Fluids and Structures 55, 526–539. doi:https://doi.org/10.1016/j.jfluidstructs.2015.04.002.

Igarashi, T., 1981. Characteristics of the flow around two circular cylinders arranged in tandem: 1st report. Bulletin of JSME 24, 323–331. doi:https://doi.org/10.1299/jsme1958.24.323.

Igarashi, T., 1984. Characteristics of the flow around two circular cylinders arranged in tandem: 2nd report, unique phenomenon at small spacing. Bulletin of JSME 27, 2380–2387.

Lin, J.C., Yang, Y., Rockwell, D., 2002. Flow past two cylinders in tandem: instantaneous and averaged flow structure. Journal of Fluids and Structures 16, 1059–1071. doi:https://doi.org/10.1006/jfls.2002.0469.

Ljungkrona, L., Norberg, C., Sunden, B., 1991. Free-stream turbulence and tube spacing effects on surface pressure fluctuations for two tubes in an in-line arrangement. Journal of Fluids and Structures 5, 701–727. doi:https://doi.org/10.1016/0889-9746(91)90364-U.

Morkovin, M., 1964. Flow around a circular cylinder – a kaleidoscope of challenging fluid phenomena. Proc. ASME Symp. on Fully Separated Flows , 102–118.

Niemann, H., 1971. On the stationary wind loading of axisymmetric structures in the transcritical reynolds number region. Konstruktiven Ingenieurbau, Ruhr-Universitat Bochum, Report .

Okajima, A., 1979. Flows around two tandem circular cylinders at very high reynolds numbers. Bulletin of JSME 22, 504–511. doi:https://doi.org/10.1299/jsme1958.22.504.

Schewe, G., Jacobs, M., 2019. Experiments on the flow around two tandem circular cylinders from sub-up to transcritical reynolds numbers. Journal of Fluids and Structures 88, 148–166. doi:https://doi.org/10.1016/j.jfluidstructs.2019.05.001.

Sumner, D., 2010. Two circular cylinders in cross-flow: a review. Journal of Fluids and Structures 26, 849–899. doi:https://doi.org/10.1016/j.jfluidstructs.2010.07.001.

Sumner, D., Price, S.J., Païdoussis, M.P., 2000. Flow-pattern identification for two staggered circular cylinders in cross-flow. Journal of Fluid Mechanics 411, 263–303. doi:10.1017/S0022112099008137.

Sun, T., Gu, Z., He, D., Zhang, L., 1992. Fluctuating pressure on two circular cylinders at high reynolds numbers. Journal of Wind Engineering and Industrial Aerodynamics 41, 577–588. doi:https://doi.org/10.1016/0167-6105(92)90467-O.

Szechenyi, E., 1975. Supercritical reynolds number simulation for two-dimensional flow over circular cylinders. Journal of Fluid Mechanics 70, 529–542. doi:https://doi.org/10.1017/S0022112075002170.

Zdravkovich, M.M., 1987. The effects of interference between circular cylinders in cross flow. Journal of Fluids and Structures 1, 239–261. doi:https://doi.org/10.1016/S0889-9746(87)90355-0.

Zdravkovich, M.M., 1997. Flow around circular cylinders, Volume 1: Fundamentals. Oxford University Press.

Zhou, Y., Alam, M.M., 2016. Wake of two interacting circular cylinders: a review. International Journal of Heat and Fluid Flow 62, 510–537. doi:https://doi.org/10.1016/j.ijheatfluidflow.2016.08.008.